December 2016

Synthesis and Characterization of Microporous and Mesoporous Zeolites from Flyash for Heavy Metal Removal from Wastewater

Saeed Golbad
University of Wisconsin-Milwaukee

SYNTHESIS AND CHARACTERIZATION OF MICROPOROUS AND MESOPOROUS ZEOLITES FROM FLYASH FOR HEAVY METAL REMOVAL FROM WASTEWATER

by

Saeed Golbad

A Thesis Submitted in

Partial Fulfillment of the

Requirements for the Degree of

Master of Science

in Engineering

at

The University of Wisconsin-Milwaukee

December 2016

ABSTRACT

SYNTHESIS AND CHARACTERIZATION OF MICROPOROUS AND MESOPOROUS ZEOLITES FROM FLYASH FOR HEAVY METAL REMOVAL FROM WASTEWATER

by

Saeed Golbad

The University of Wisconsin-Milwaukee, 2016
Under the Supervision of Professor Nidal Abu-Zahra

Class F fly ash was hydrothermally modified in one- and two-step processes to prepare zeolites with enhanced adsorption characteristics. Highly crystalline X type zeolite and hydroxy sodalite were targeted as microporous and mesoporous zeolite and were successfully synthesized using fly ash precursor by adjusting Si/Al molar ratio in reaction mixture. The heavy metal removal performance of the obtained fly ash-based zeolites was investigated in batch Pb^{2+} adsorption experiments.

Lead (Pb^{2+}) is a positively charged toxic pollutant that can be present in surface water and industrial wastewater and may cause harmful physiological effects to human. As a result, standards for water quality are becoming increasingly stringent. This has accelerated the development of innovative, cost effective adsorbent during recent years.

Since zeolites have an inherent negative charge in their framework, they are capable of removing heavy metals from water. This study explores economical alternatives of removing positively charged contaminants using fly ash-based zeolites. Zeolites are a class of porous aluminosilicates with high cation exchange capacity. Fly ash has large amounts of silica and alumina in its composition and is a suitable precursor for synthesis of a wide variety of zeolites with enhanced adsorptive characteristics.

The hydrothermally synthesized zeolites were subject to instrumental characterization. The ammonium acetate saturation method followed by atomic absorption spectroscopy was employed for cation exchange capacity measurements. The presence of porosity, as well as high specific surface area (as high as 424 m^2/g) and exchange capacity (as high as 320 meq/g) suggest potential applications for the hydrothermally synthesized zeolites in adsorption and ion exchange applications.

The removal of Pb^{2+} with hydroxy sodalite and Na-X zeolite was investigated under various conditions. The adsorption capacity of hydroxy sodalite increased with an increase in contact time, and a 98.1% removal efficiency was seen for a solid/liquid ratio of 3.0 g/L, pH=5.5 and an initial lead concentration of 100 mg/dm^3. The Langmuir model represented lead adsorption using sodalite better than the Freundlich model and the maximum adsorption capacity of Pb^{2+} onto hydroxy sodalite was 153.8 mg/g. The results indicate that Pb^{2+} can be adsorbed successfully in significant amounts on the modified fly ash.

Kinetic and isotherm studies were conducted to investigate the potential of Na-X for the removal of lead from aqueous solution. The effect of initial pH on adsorption process was investigated and kinetic equations were used to model experimental data. Based on the kinetic experiments, the equilibrium time required for the adsorption of lead from aqueous solution by Na-X under different pH conditions was evaluated. The pseudo second order model represented the adsorption kinetics better than the pseudo first order model. The reaction rate constants, as well as sorption capacity increased with increasing pH in the range of 3 to 6. Optimum pH for the removal of lead was found to be 6.0.

TABLE OF CONTENTS

LIST OF FIGURES

LIST OF TABLES

ACKNOWLEDGEMENTS

I am deeply grateful to my thesis and academic advisor, Professor Nidal Abu-Zahra, for his guidance, support, encouragement, and trust. I have benefited from his open-minded approach to new ideas, his high standards of accomplishment, and his philosophy of research.

I would like to express my appreciation to my thesis committee members, Professor Ben Church, and Professor Steve Hardcastle, for their valuable discussions and helpful suggestions.

Finally, and most importantly, I wish to express my deepest gratitude to my parents and sisters for their unfaltering love and support, the values they instilled in me, and their encouragement during my whole life. For her love, support and motivation, I dedicate this thesis to my wife, Parisa.

Chapter -1) Introduction to zeolites

Zeolites are a class of naturally occurring and synthetically produced, crystalline aluminosilicate minerals with three-dimensional structures which arise from oxygen linked framework of $[SiO_4]^{4-}$ and $[AlO_4]^{5-}$ polyhedral. They are capable of reversible and facile cation exchange. The structure of tetrahedral form a porous matrix with regular array apertures having defined dimensions and therefore able to selectively admit some molecules into their interiors while rejecting others on the basis of molecular dimensions and giving them the important property of molecular sieving (Barrer 1985, Cundy and Cox 2005, Maesen 2007, Ribeiro 2012).

The fascinating properties of zeolite materials, such as their ion-exchange properties, their sorption capacity, their shape selectivity, their catalytic activity, or their role as hosts in advanced materials, are determined by their crystal structure. Sorption characteristics depend upon the size of the pore openings and the void volume and ion-exchange selectivity upon the number and nature of the cation sites and their accessibility. Therefore, an important aspect of zeolite science is structural analysis (Auerbach, Carrado et al. 2003, Weitkamp and Puppe 2013, Mitchell, Pinar et al. 2015).

The ion exchange and molecular sieving properties have resulted in commercialization of natural and synthetic zeolite adsorbents and has made them a strong prospect for heavy metal removal from industrial wastewater. Production of zeolites from fly ash offers the opportunity to create an added value product from an industrial waste (Auerbach, Carrado et al. 2003, Ahmaruzzaman 2010, Barakat 2011, Ribeiro 2012, Xie, Wang et al. 2013).

Most studies on heavy metal removal using zeolites have been performed using naturally occurring zeolites, such as clinoptilolite, chabazite and mordenite to provide basis for the performance comparison. The flexibility of increasing cation exchange capacity and metal adsorption capacity is restricted by topology and structure that are both defined by natural processes and have limited scope for modification. Natural zeolites also have limitations in heavy metal uptake, whereas fly ash-based

synthetic zeolites possess a variety of pore structures and are potential sorbent minerals for trapping various contaminants from air and water. Synthetic routes offer flexibility in controlling topology of zeolite, cation type within the zeolite framework, pore size distribution and particle size. (Erdem, Karapinar et al. 2004, Wang and Peng 2010, Margeta, Farkas et al. 2013, Koshy and Singh 2016).

The objective of this study is to analyze silicon extraction from fly ash and crystallization of zeolites capable of efficient removal of heavy metals from wastewater effluents. Synthetic routes allow the enhancement and optimization of metal adsorption capacity and selectivity. Using a combination of characterization techniques and solution characterization (Atomic Absorption Spectroscopy) methods, the effect of synthesis variable on the structure of the resulting fly ash-based zeolite and its influence on heavy metal uptake will be explored.

1.1) Aims and Objectives

This thesis will explore the feasibility of a sustainable, low cost, high-performance technology used in water treatment, geared specifically towards industries that require treatment of controlled or uncontrolled discharges of waste. The goal of the study is to develop innovative materials and method with significant commercial potential for removing heavy metals from water. This includes investigation and optimization of a process for the production of high performance adsorbents from industrial coal burning by-product. Another objective is to characterize the mineral, textural, morphological, and chemical properties of thus obtained zeolite products and improve operating parameters for efficient removal of heavy metal ions. This work includes an investigation of the regenerative properties of the adsorbents suitable for treatment of large amounts of heavy metal-contaminated water and the possibility of incorporation of the materials into point-of-use devices.

1.2) Fly Ash, Production and Uses

Fly ash is by-product of coal burning process generated in coal thermal power plants, Fly ash is defined as “fine-grained powder, which is mainly composed of spherical glassy particles, produced during the combustion of pulverized coal” by British standard EN 450-1:2012 (EN 2012). Coal combustion produces two main solid by-products: bottom ash, and fly ash. Fly ash forms between 60 and 88% of the solid residue and has been regarded as problematic industrial solid waste. The ash is composed of different types of particles with different size, composition and morphology. In order to meet emission standards and reduce the harm to the environment, fly ash is removed from the flue gas, either by filtration using bag filters, cyclones or electrostatic precipitators. The estimated global production of fly ash is 750 million tones (Wdowin, Franus et al. 2014, Zhou, Chen et al. 2014, Bukhari, Behin et al. 2015, Yao, Ji et al. 2015).

Fly ash is used as an aggregate and structural fill, such as landfill and roadbeds. Other applications involve some treatment of the fly ash in brick manufacture, ceramics, catalysts and catalyst support, adsorbent for gas streams or organic compounds, chemical fertilizer, and Chemical Oxygen Demand (COD) reducer. Due to fine particle size and proper binding properties, fly ash is used as a replacement for pozzolanic material in Ordinary Portland Cement (OPC). It also has application as filler in polymer industry, and has been perceived as an exceptional precursor for synthesis of molecular sieves due to high content of silica and alumina in its composition (Shih and Chang 1996, Chang, Chun et al. 1999, Wang, Guo et al. 2003, Wdowin, Franus et al. 2014).

The components of fly ash are mainly alumina, silica, and calcium oxide. The physical features of fly ash, including bulk density, porosity, and surface characteristic, make it an economical alternative for conventional adsorbents. One of the advantages of using fly ash in wastewater treatment is its ease of solidification after metal adsorption. Many studies are reporting on raw fly ash adsorbents for heavy metals removal from wastewater. Variability of composition, mineralogy, and morphology of different fly

ash samples hinders their direct use. Indirect application of fly ash usually involves a series of chemical, thermal, and mechanical processes in order to improve the desired properties (Ahmaruzzaman 2010, Blissett and Rowson 2012, Bandura, Franus et al. 2013).

The new concept, “waste for waste treatment” is now largely being applied for wastewater treatment using solid wastes resulted from coal combustion process. However, fly ash exhibits lower adsorption capacity compared with that of the traditional adsorbent. An economic and efficient activation method can convert fly ash into zeolites. The adsorption performance of zeolites is much better than that of fly ash, thus the development of performant zeolite adsorbents using fly ash have been a route more recently investigated (He, Chen et al. 2016, Koshy and Singh 2016, Visa 2016).

1.3) Introduction to zeolites

Zeolites (Greek, zein, "to boil"; lithos, "a stone") are the oldest and the largest group of microporous materials widely known as “molecular sieves”. They are crystalline inorganic polymers, or better said, three-dimensional porous aluminosilicates, consisting of 3-dimensional arrangement of $[SiO_4]^{4-}$ and $[AlO_4]^{5-}$ polyhedral connected through their oxygen atoms to form a negatively charged lattice due to isomorphous substitution of Si^{4+} by Al^{3+}. In order to maintain electro-neutrality, mobile counter-cations are stored in the intravoidal water of the zeolite solid (Chunfeng, Jiansheng et al. 2009, Ribeiro 2012, Weitkamp and Puppe 2013, Wdowin, Franus et al. 2014). General formula of zeolites are expressed in Equation (below)

$$M_{\frac{x}{n}}\left[(AlO_2)_x.(SiO_2)_y\right].w(H_2O) \qquad \textit{Equation 1-1}$$

Where M is a cation of valence n that balances the negative charges associated with the aluminum tetrahedral, the terms x and y correspond to the stoichiometric coefficients of the alumina and silica tetrahedral and w is the number of water molecules.

Zeolites have an open structure that accommodates a variety of cations, such as Na^{+}, K^{+}, Ca^{2+}, and Mg^{2+}, as well as mobile water molecules that can be readily lost and regained, accounting for their desiccant properties. The loosely bound positive ions can be readily exchanged for others in aquatic environment. This gives the porous structure ability of ion-exchange. The ratio of silica to alumina commonly varies between one and five, giving different framework compositions (Barrer 1985, Marcus and Cormier 1999, Ribeiro 2012). Idealized structure of zeolite framework is presented in Figure 1-1 Idealized structure of zeolite - Si/Al substitution yielding a negative charge on framework (Querol, Moreno et al. 2002).

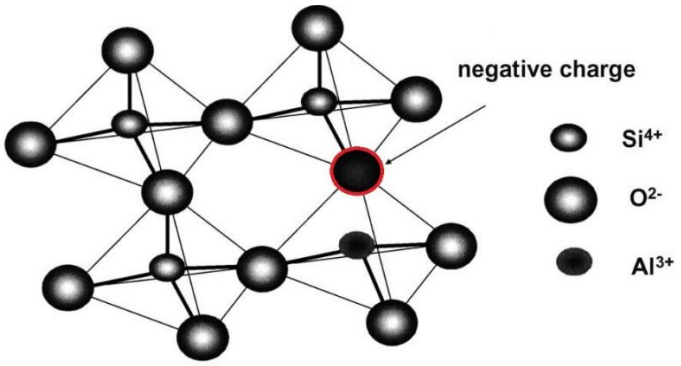

Figure 1-1 Idealized structure of zeolite - Si/Al substitution yielding a negative charge on framework (Querol, Moreno et al. 2002)

Zeolites have valuable physiochemical properties, such as adsorption, cation exchange, molecular sieving, and catalysis. The wide variety of applications includes separation and recovery of normal paraffin hydrocarbons, catalysis of hydrocarbon reactions, drying of refrigerants, separation of air components, removing carbon dioxide and sulfur compounds from natural gas, separating hydrogen isotopes, and removing heavy metal ions from industrial wastewaters (Maesen 2007, Qiu and Zheng 2009, Yadanaparthi, Graybill et al. 2009, Franus and Wdowin 2010, Zhao, Wu et al. 2010, Weitkamp and Puppe 2013, Cardoso, Paprocki et al. 2015).

1.4) Natural and Synthetic zeolites

Natural zeolites are used in water treatment, aquaculture, paper manufacturing, gas adsorption and chemical catalysis. However, they have restricted pore sizes and channels, whereas synthetic fly ash-based zeolites can be tailored to possess a variety of pore structures and are economically viable sorbents for air and water decontamination. Zeolites synthesized from fly ash has been reported to have 6-7 times higher lead sorption capacity than raw fly ash and 3-5 times higher than natural zeolites (Erdem, Karapinar et al. 2004, Margeta, Farkas et al. 2013, Bandura, Franus et al. 2015, Yao, Ji et al. 2015, Koshy and Singh 2016).

Synthetic zeolites are produced from a variety of high-Si and Al starting materials. Zeolitic materials are highly selective scavengers of a variety of heavy metals from liquid effluents through the process of ion exchange. The sorption capacity of synthetic zeolites can be superior to their natural counterparts; therefore, synthetic zeolites have a clear advantage over natural alternatives in adsorption application (Auerbach, Carrado et al. 2003, Ribeiro 2012, Bandura, Franus et al. 2015, Grela, Hebda et al. 2016).

1.5) Microporosity and mesoporosity of zeolites

Micro and mesoporous solids have attracted considerable interest in the field of water treatment, because of their large surface area and extremely high porosity. Microporous materials have a pore diameter less than 2 nm and mesoporous materials have a pore diameter ranging from 2-50 nm. The term nanoporous materials have been used for porous materials with a pore diameter of <100 nm whether or not the structure itself is nano size. They are able to interact with species both on their outer surface and throughout their inner porous network, giving them a huge potential for applications in a variety of fields. They can selectively sort molecules based on their size (Cundy and Cox 2005, Jha and Singh 2014, Grela, Hebda et al. 2016).

High porosity synthetic zeolites have been popular materials since their advent in late 1940s for catalysis, separation and purification applications, among others. They have a highly ordered structure and offer a unique advantage of narrow pore size distribution. Zeolites function on the basis of physisorption. The main driving force of the adsorption is the highly polar internal surface of the zeolite. This unique property distinguishes zeolites from other adsorbents and enables them to have an extremely high adsorption capacity. Maintaining a charged and large internal surface area, having a defined aperture size, and presence of pores and cavities in the order of molecular dimensions (0.3-1.0 nm) plays a significant role in separation process, allowing or prohibiting the entrance of molecules to the pore system, leading to catalytic properties and high separation factors (Barrer 1985, Querol, Moreno et al. 2002, Barakat 2008, Belviso, Cavalcante et al. 2014).

The unique structure of zeolites allows the water of crystallization to be removed, leaving a porous crystalline structure. These pores or cages have a high affinity to absorb water or other polar molecules. Molecules with large polarity or polarizability can be preferentially adsorbed under identical conditions. The application of zeolites as molecular sieve and catalyst depends on size and shape of their channel systems, as well as the nature and location of cations in framework. The connection of SiO_4 and AlO_4 forms a variety of secondary structural units, which in turn are linked to form inorganic macromolecules with specific crystal structure (Ribeiro 2012, Shoumkova and Stoyanova 2013).

The use of fly ash for zeolite synthesis and determination of heavy metal uptake is crucial for creating water treatment solutions for regions having limited water resources. Some common zeolites synthesized from fly ash are presented in Table 1-1. Fly ash-based zeolites have been reported to have higher lead sorption capacity than raw fly ash (6–7 times) and natural zeolites (3–5 times) (Lee, Yi et al. 2000, Zabochnicka-Świątek and Malińska 2010). Synthesis of chemical structures with exceptionally large surface area and controlled pore sizes is a great challenge in materials research.

Table 1-1 Some common zeolites synthesized from fly ash

Zeolite	Chemical formula	References
Na-A	$Na_{12}Al_{12}Si_{12}O_{48}.24H_2O$ $NaAlSi_{1.1}O_{4.2}.2.225H_2O$	(Adamczyk and Bialecka 2005, Qiu and Zheng 2009)
Na-P1	$Na_6Al_4Si_4O_{24}.4H_2O$ $Na_6Al_6Si_{10}O_{32}.12H_2O$	(Qiu and Zheng 2009, Cardoso, Paprocki et al. 2015, Deng and Ge 2015)
Zeolite X	$NaAlSi_{1.23}O_{4.46}.3.07H_2O$	(Qiu and Zheng 2009)
Zeolite Y	$NaAlSi_{2.43}O_{6.86}.4.46H_2O$	(Qiu and Zheng 2009)
Phillipsite	$(Ca,Na_2,K_2)_3Al_6Si_{10}O_{32.12}H_2O$	(Hay 1966)
Mordenite	$(Ca, Na_2, K_2)Al_2Si_{10}O_{24.7}H_2O$	(Sasaki, Oumi et al. 2003)
Sodalite	$Na1.08Al2Si_{1.68}O_{7.44}.1.8H_2O$	(Golbad, Khoshnoud et al.)
Clinoptilolite	$(Na,K,Ca)_{2\text{-}3}Al_3(Al,Si)_2Si_{13}O_{36}.12H_2O$	(Zabochnicka-Świątek and Malińska 2010)
Chabazite	$(Ca,Na_2,K_2,Mg)Al_2Si_4O_{12}.6H_2O$	(Dedecek, Sklenak et al. 2009)
Cancrinite	$Na_6Ca_2Al_6Si_6O_{24}(CO_3)_2.2H_2O$ $Na_{14}Al_{12}Si_{13}O_{51}.6H_2O$	(Qiu and Zheng 2009)

1.6) Characterization of zeolites

Usually, a number of analytical techniques are combined to examine the structure of a zeolite. This includes sorption experiments, solid state NMR, electron microscopy and powder diffraction. The applicability of zeolites is linked with their crystalline architecture and clear understanding of the structure of zeolites is vitally important for understanding their properties. The most powerful method of obtaining long-range structure of crystalline materials uses diffraction of radiations with a wavelength in the same order of magnitude as the distance between atoms in the structure (0.1-0.2 nm). X-rays are the

most widely used radiation for this type of work. The types of information obtained by diffraction experiments on zeolites range from the relatively simple identification of a known phase from its diffraction "fingerprint" to more advanced refinement techniques to obtain structural models and some properties such as average particle size for a zeolite (Auerbach, Carrado et al. 2003, Terasaki, Ohsuna et al. 2007).

1.7) Zeolite framework types and characteristics

A framework type describes the connectivity of the tetrahedrally coordinated atoms of the framework in the highest possible symmetry. Therefore, many different materials can be classified under one designation. A three-letter code is assigned to confirmed framework types by the International Zeolite Association. The codes are normally derived from the name of the zeolite, e.g. FAU from the mineral faujasite, and LTA from Linde Type A. Description of a zeolite structure mostly begins with a description of framework type in terms of pore opening size and dimensionality of the channel system. Pore openings are characterized by the size of the ring that defines the pore, designated an n-ring, where n is equal to the number of T atoms (tetrahedrally coordinated cations) and O-atoms in the ring. An 8-ring is considered an small pore opening, a 10-ring being medium and a 12-ring a large one with effective pore width of 0.41, 0.55, and 0.74 nm, respectively (calculated using an oxygen radius of 0.135 nm).

Some structural features (cages, channels, chains and sheets) are common to several different zeolite frameworks. Some of these subunits are shown in Figure 1-2. For example, sodalite cage is a truncated octahedron whose surface is defined by six 4-rings and eight 6-rings, therefore sodalite would be designated as $4^6 6^8$ cage (Auerbach, Carrado et al. 2003, Xu, Pang et al. 2009, Ribeiro 2012).

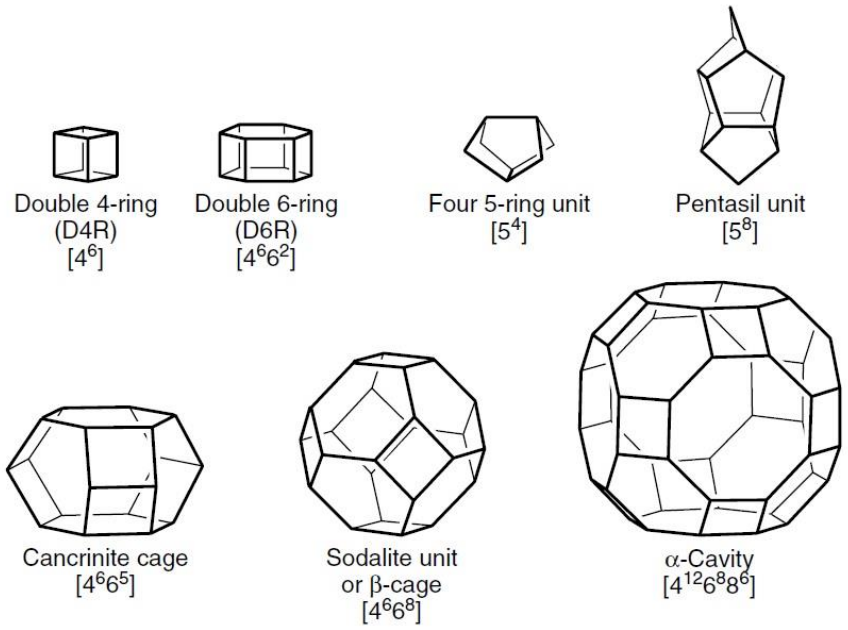

Figure 1-2 Some subunits and cavities seen in many framework types

The stacking sequence of layers, cages, or rings in zeolite frameworks is often described using "ABC-system". This terminology for crystal chemistry is normally used to describe the stacking of layers of closest packed spheres (atoms). This concept is not only a way to describe a family of frameworks, but also reflects the way nature builds real materials with such frameworks (Auerbach, Carrado et al. 2003, Baerlocher, McCusker et al. 2007).

Although there are 232 confirmed zeolite framework types (as of 2016), only a few of them describe zeolites that are used in industrial applications. Sodalite (SOD) is an important material for creating simple periodic arrays of clusters, and one of the most important hosts for advanced materials. The best description of SOD framework is " a body centered cubic arrangement of β- or sodalite- cages joined through shared 4- and 6-rings" and can be viewed as an ABCABC stacking of hexagonal arrays of single 6-rings in the [111] direction (Figure 1-3).

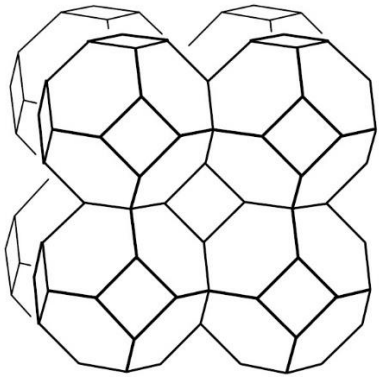

Figure 1-3 The SOD framework type

The LTA framework type consists of primitive cubic arrangement of sodalite cages via oxygen bridges to form double 4-rings. This creates an α-cavity and a 3-dimensional 8-ring channel system, instead of β-cage in the center of the unit cell (Figure 1-4). Zeolite A is a technologically important porous zeolite which is widely used for various separation and purification applications it is used as a desiccant and as an ion-exchanger (water softener) in laundry detergents.

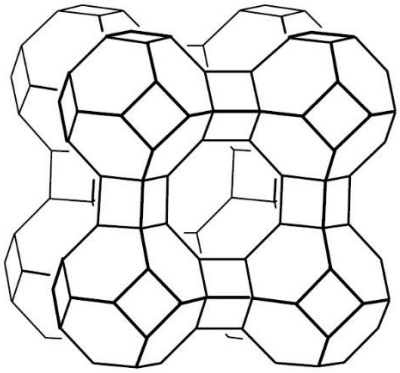

Figure 1-4 The LTA framework type

Zeolite A in its as-synthesized form (molecular sieve 4A) has the unit cell formula, $Na_{12}(AlO_2)_{12}.nH_2O$. Sodium ions can be exchanged by calcium, silver, potassium or other metal ions to yield adsorbents with desired properties for different applications. The state, number and location of cations in framework have significant influence on adsorption properties of the zeolite. Exchange of Na^+

ions in molecular sieve Na-A with Ag^+ ions will reduce the pore opening further and causes antimicrobial activity.

1.8) Anionic nature of Zeolite Framework

The fact that zeolite framework is anionic and balancing cations are exchangeable is the reasons behind many of the interesting zeolite properties. Pure silica (SiO_2) framework is neutral in nature. If some of the tetravalent Si atoms are replaced by trivalent Al to produce an aluminosilicate, the framework becomes negative and would need balancing counterions such as Na^+. The framework composition defines the stability of the material. A high-silica zeolite generally has a higher thermal stability than a corresponding aluminosilicate with high aluminum content.

Cost-effective production of zeolites from fly ash provides an opportunity for effective and value added management of fly ash. Hydroxy Sodalite ($Na_8[AlSiO_4]_6(OH)_{2.2}H_2O$) is one of the interesting sodalite family members with a small aperture size. The material can be an ideal candidate for the separation of small molecules and ions from mixtures. A customized zeolite synthesis offers many advantages over mining and processing natural zeolites, such as higher ion affinity.

1.9) Structural details and classification of zeolites

Properties of zeolites are dependent on the topology of its framework, the size, shape, and accessibility of its free channels, the charge, and size of the cations within the framework, the ordering of the tetrahedra and the local environment of T-atoms. The fundamental building block of all zeolites is a tetrahedron of four oxygen anions surrounding a small silicon or aluminum ion. Variations in framework architecture and cation exchange capabilities produce a family of materials, with specific selectivity and sieving properties. The alumina and silicate tetrahedra are known as primary building units, and corner-share oxygen, combining to form a number of different basic structures called Secondary Building Units (SBU's), and these SBU's link to form a three dimensional lattice. The SBU's are named according to the

size of the "oxygen windows" which determine the geometry of the cavities and channels formed in the framework.

Zeolites can be classified according to their structure type, each particular structure type is assigned a structure code, relating to its topological category and referred to as a three-letter abbreviation. It is possible for two zeolites of exactly the same chemical composition. In addition, zeolites of the same structure class can have different chemical compositions, varying both in silicon-to-aluminum ratio (Si:Al) and the nature of the exchangeable cations. The cationic form of the zeolite is usually described by prefixing the elemental symbol to the zeolite name.

Zeolites can also be differentiated by their networks of cavities and interconnecting channels. In some zeolites the channels can run parallel to a single direction, and these zeolites are known as fibrous or chain zeolites. Common examples are edingtonite and natrolite. These zeolites consist of sheets of chains, formed when the tetrahedra share only one oxygen, with channels running in a single direction.

In lamellar zeolites, only three corners of each tetrahedron are shared, hence the zeolite channels run parallel to two perpendicular axes. This structure is commonly found in phillipsite and other sedimentary zeolites. If all four corner oxygen atoms of the tetrahedral are shared, then the most common zeolite structure is formed, with the zeolite channels running parallel to three dimensional cubic axes.

Conventionally, zeolite frameworks comprise of interconnecting channels and cavities, within which exchangeable charge-balancing cations are stored. Exchange and catalytic activity occurs within these channels rather than primarily in the large cavities found in more conventional zeolite forms such as zeolite A.

1.10) Synthesis and formation of zeolites

The first synthetic zeolite was made in 1862 by St. Clair Deville who reported the production of levyne (levynite) by heating potassium silicate with sodium aluminate in a sealed glass tube. The first

synthesis involving complete characterization of a new zeolite structure (Zeolite A) was carried out at the Union Carbide Laboratories, by Milton and coworkers.

Synthetic zeolites have many advantages over their natural counterparts. Zeolites type A, X, Y, P and Na-P1 are well known synthetic zeolites with a wide range of industrial applications. The starting point of zeolite synthesis is crystallization from an amorphous gel formed upon mixing the reactants - caustic aluminate solution and caustic silicate solution. The crystallization is typically carried out in a batch reactor, where the temperature is maintained at a level above ambient (60-180°C) and at autogenous pressures for a period of time ranging from hours to days. After nucleation, zeolite crystals grow larger by assimilation of aluminosilicate material from the solution phase. This is driven by the dissolution of the amorphous gel to replenish the solution with aluminosilicate species. The first step involves:

1) Primary nucleation (homogeneous and heterogeneous), and

2) Secondary nucleation (initial breeding, contact, shear, attrition).

Primary nucleation is driven by the solution, in the absence of crystalline phases either strictly within the solution as in the case of homogenous nucleation, or catalyzed by extraneous material/surface in the solution that reduces the energy barrier for formation of crystalline phases, as in the case of the heterogeneous nucleation. With the presence of amorphous gel in most zeolite synthesis systems, the heterogeneous nucleation on gel surfaces is considered significant in describing mechanisms of zeolite nucleation.

Secondary nucleation is catalyzed by the presence of parent crystals of the same phase, and occurs with lower activation energy than primary nucleation. The parent crystals might be added as seed crystals at the beginning of a synthesis (initial breeding), or grown in the original unseeded system. In the absence of seed crystals added to the solution, agitation could sometimes promote nuclei generation by crystal contact with a stirrer (contact), by action of fluid contact at sufficient velocities with a growing

crystal (shear) or simply by means of a random event (micro-attrition), where microcrystalline fragments are broken off existing growing crystals. The dominating effects of one or more of these mechanisms depend upon the processing conditions.

Adding seed crystals to a crystallization system results in increased crystallization rates due to an increase in the rate at which solute can integrate with the solid phase from solution on account of higher available surface area and also due to the enhanced nucleation of new crystals.

Zeolite crystal growth from solution occurs by transfer of material from the solution phase, in which the solute has three-dimensional mobility, to the surface of the crystal lattice being formed, and incorporation into a regularly ordered framework. Thus, individual species must diffuse to the crystal structure, and then be incorporated into the crystalline structure for growth to occur, as measured by the advancement of the crystal faces, or the increase in the crystal dimensions. Consequently, it is possible that either solute diffusion or surface kinetics may be rate controlling. This suggests a surface kinetics limited crystal growth rather than diffusion limited growth, where the incorporation of solute by surface integration kinetics dominates over the solute transport through the liquid layer.

Synthetic zeolites are conventionally synthesized by silicate and aluminate solutions in alkaline conditions at temperatures between 100°C and 200°C. A gel phase is precipitated, which will gradually dissolve and re-precipitate with time, leaving zeolite and various side products. This chain of reactions is known as Ostwald's rule of successive transformations, which states that as each successive phase appears, it will be thermodynamically more stable than its predecessor was. It is known that the temperature, pressure, pH, chemical composition, and nature of the reactant solutions all affect the synthesis process. Relative concentrations of silicate and aluminate are important parameter that can never fall below 1.0, since Loewenstein's rule prevents the formation of an Al-O-Al linkage within the zeolite framework. The addition of specific template cations or salts can aid synthesis of specific zeolite structures by allowing the structure to form around the template ion.

Upon activation of fly ash using alkalis, such as NaOH, KOH, $Ca(OH)_2$, and $Li(OH)_2$, dissolution and crystallization processes are performed to synthesize zeolite phases. The main synthesis methods are (Sasaki, Oumi et al. 2003, Adamczyk and Bialecka 2005, Cundy and Cox 2005, Somerset, Petrik et al. 2005, Nascimento, Soares et al. 2009, Belviso, Cavalcante et al. 2014):

- Conventional hydrothermal treatment
- Alkali fusion-assisted hydrothermal
- Microwave-assisted hydrothermal
- Ultrasonic-assisted hydrothermal
- Molten salt method

Alkali fusion-assisted hydrothermal and molten salt methods were selected for the activation of fly ash in this study.

1.11) Pore Size Modification

The size of the pore windows can be modified by altering the silicon to aluminum ratio of the zeolite framework during synthesis. This will change the charge density and exchange capacity of the zeolite. The higher the Si/Al, the lower the number of exchangeable cations located in the pore windows, and the wider the window diameters. Increasing the silicon to aluminum ratio will also increase the hydrophobicity of the zeolite, leading to the ability to selectively absorb organic compounds dissolved in water. The type of cation can also be altered, either by exchanging for ions of smaller radii or one divalent ion for two monovalent ones. Additionally, changing the cation may also change the location of the exchangeable ion since different exchange sites have different affinities.

1.12) Adsorption process

Each metal has a tendency to form specific compounds in water and the dissolved meal can be removed by different mechanisms, mainly adsorption and ion exchange. Adsorption is a surface phenomena involving the adhesion of atoms, ions, or molecules of gas, liquid, or dissolved solid to a

surface that forms a molecular or atomic film. Desorption is the reverse of adsorption process. The term sorption encompasses both adsorption and absorption. The adsorbing species is called the adsorbate and the solid media to which the sorbate is attracted is known as the adsorbent. The main factors influencing sorption process are:

- Adsorbent characteristics
- Adsorbate properties
- Reaction environment

In water treatment applications, adsorbents can be used in the form of pellets, rods, moldings, or monoliths. Composition and structure of adsorbent define its sorption capacity. The most important characteristics affecting the sorption capacity of an adsorbent are surface area, surface charge, and stability (thermal and chemical).

The sorption capacity increases with the increase of specific surface area and the surface charge determines the affinity toward either cations or anions. Negative surface charge provides sites for cations. Poor thermal or chemical stability can limit the operating conditions for ion exchange or regeneration processes. The adsorbate properties affecting the sorption capacity include concentration level, chemical form, water solubility, and hydration energy (Wu, Sui et al. 2008, Izidoro, Fungaro et al. 2013, Pathania, Singh et al. 2013).

Heavy metals exist in water in dissolved form, colloidal and particulate forms. The soluble forms are mostly ions or unionized organometallic complexes. Sorption of heavy metals in water is controlled by reaction environment characteristics, such as pH, redox potential, ionic strength and competing ions. The efficiency of adsorption is mainly determined by the type of adsorbate but also exposure time, dosage, and efficiency of preliminary water treatment. Exposure time depends on water temperature and the type of activated bed.

The proper selection of technical solutions for the contact of adsorbate with water is affected by the form of adsorbent. Adsorbents in powder form can be added to raw water during coagulation or before filtration. They can also be added to the high rotation stirred chambers or before settling tanks equipped with a suspended bed. The addition of an adsorbent improves the sedimentation properties of agglomerates formed during the process of flocculation.

Grainy or granular adsorbents can be applied in flow-through systems as a layer in multilayer filtration/sorption beds. In order to reduce the dose of an adsorbent and also to minimize the exposure time of water and an adsorbent, it is sometimes necessary to identify the best dosing point for each system. The main criteria for choice of an adsorbent for heavy metal removal from water are:

- Metal adsorption must be thermodynamically possible.
- The kinetics of adsorption process must be fast.

The effectiveness of heavy metal removal by zeolites depends on the concentration of ions in solution and type of the metal ions to be removed. The zeolitic material must be added in sufficient amount to adsorb the heavy metal content of water. Synthetic fly ash-based zeolites have many potential applications in environmental protection. The type of fly ash used in the synthesis, method, temperature and solution/fly ash ratio determine the type of zeolite of different structure and efficiency.

Ion exchange can remove heavy metals from solution by exchanging a mobile ion in an aqueous or gaseous phase with an exchangeable ion of the same charge in an adsorbate framework. This reaction is reversible, and preferential exchange can occur with other mobile ions in the environment. Multivalent ions tend to be more strongly attracted to sites of opposite charge. Although ion exchange reactions have been studied extensively, it is only fairly recently that the application of these materials to wastewater treatment has been considered.

The ion exchange process consists of a number of distinct stages, which are represented in Figure 1-5. Ion diffusion through the thin film on the surface of the ion exchange material and through the matrix itself are frequently the rate limiting steps, as the ion exchange reaction itself is very rapid.

The ion exchange reaction should be considered a bulk phase interaction rather than a surface phenomenon, since the exchange occurs within the internal pores and channels of the zeolite particle rather than on the particle surface. During a binary ion exchange reaction, a mobile ion in an aqueous or gaseous phase (M_A) is exchanged with an exchangeable ion (M_B) in the zeolite framework. This exchange can be simply expressed as:

$$\overline{z_A M_B} + z_B M_A \leftrightarrow z_A M_B + \overline{z_B M_A} \qquad \text{Equation 1-2}$$

Where the zeolite phase is denoted by a bar. The respective valences of the two ions are Z_A and Z_B. This reaction is reversible, and preferential exchange can occur with other mobile ions present. Multivalent ions (trivalent and above) tend to be more strongly attracted to sites of opposite charge. Different steps of ion-exchange process from a mass transfer point of view are depicted in Figure 1-5.

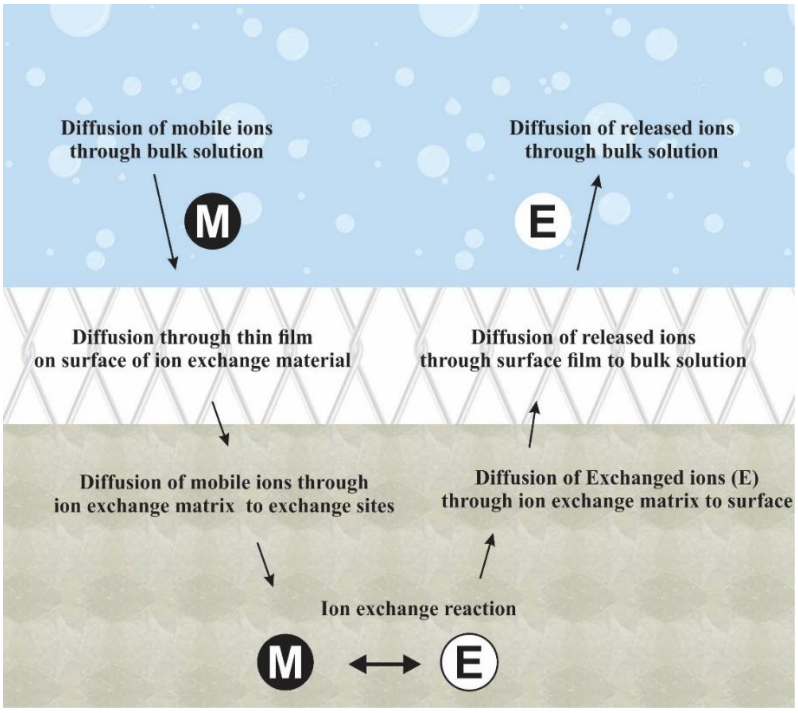

Figure 1-5 Schematic illustration of the ion exchange process

1.13) Ion Exchange Equilibria

It is beneficial to be able to predict ion exchange equilibria and selectivity from experimental data. Some parameters are difficult to measure experimentally and these can be derived by calculation from their relationships with other, more easily established parameters. In a binary system, the separation factor (α) can be derived from the following equation:

$$\alpha = \overline{E_A}E_B / \overline{E_B}E_A \qquad \text{Equation 1-3}$$

Where E_A is the equivalent fraction of cation M_A in the solution phase and correspondingly E_B for the cation M_B, with the zeolite phase indicated by the bar. The respective equivalent fractions can be calculated from below equations:

$$E_A = z_A.n_A/(z_A.n_A + z_B.n_B)$$ Equation 1-4

$$\overline{E_A} = z_A.\overline{n_A}/(z_A.\overline{n_A} + z_B.\overline{n_B})$$ Equation 1-5

n_A and n_B represent the moles per unit volume of the cations M_A and M_B within each phase. The separation factor can be derived from ion exchange isotherms. These are graphs, determined experimentally at constant temperature and total solution normality, or the equivalent fraction of an exchangeable ion in the zeolite phase (x-axis) against the equivalent fraction in solution (y-axis). The separation factor can be determined graphically as the area above the isotherm curve divided by the area below the curve.

Thermodynamic parameters can be developed from the isotherm data. The mass action quotient (k_m) can be calculated from the following relationship:

$$K_m = ({m_b}^{z_A}.\overline{{E_A}^{z_B}})/({m_A}^{z_B}.\overline{{E_B}^{z_A}}$$ Equation 1-6

Where m_A and m_B are the molal concentrations of cations M_A and M_B (mol/kg). Additionally the thermodynamic equilibrium constant (k_a) can be derived from equation below:

$$K_a = ({a_B}^{z_A}.\overline{{a_A}^{z_B}})/({a_A}^{z_B}.\overline{{a_B}^{z_A}})$$ Equation 1-7

With the "a" parameters representing the activities of cations M_A and M_B in the solid and solution phases (mol/l). The thermodynamic equilibrium constant is a function of the activities, whilst the mass action quotient is defined with respect to cation concentrations, and they are connected by the following expression:

$K_a = K_m.\Gamma.\Phi$ Equation 1-8

With Γ defined as an activity correction coefficient for the solution phase, and Φ as the activity correction coefficient for the zeolite phase. A corrected selectivity coefficient (k_G) can be determined from:

$K_G = K_m.\Gamma$ Equation 1-9

The standard Gibbs energy of exchange (ΔG) (J/mol) can be calculated from Equation 2.15.

$\Delta G = -(\frac{RT}{z_A z_B}).\ln k_A$ Equation 1-10

1.14) Ion Exchange Capacities

Ion exchange capacities are valuable from a practical standpoint. The exchangeable ions of a zeolite are cations associated with the aluminum tetrahedra of the zeolite framework. These ions are available for exchange with cations from the bulk solution. The total exchange capacity is a measure of the density of fixed charges within the zeolite framework, calculated from the aluminum content of the zeolite.

The cation exchange capacity refers to the equivalents of exchangeable cations per unit quantity of the zeolite. This can be classified as theoretical exchange capacity, or effective exchange capacity. CEC values are usually reported in meq/100gr, or meq/g units.

Theoretical exchange capacity of a zeolite refers to its maximum cation exchange level and is expressed as the total amount of cations in a specific quantity of the material. It depends solely on the aluminum content in the zeolite and can be increased by lowering Si/Al ratios in the zeolite through synthesis routes. Of practical interest is the effective capacity, which refers to the amount of exchangeable cations contained in a specific quantity of the zeolite under specific experimental conditions. The difference between the theoretical and effective exchange capacities arises because some of the zeolite cations have low mobility or are strongly bound within the structure of the material and thus, cannot easily be removed. Hence, effective exchange capacity is always lower than theoretical exchange capacity.

To maintain electro-neutrality, all fixed charges must be balanced. In practice, this is rarely achieved, and the operating capacity of a zeolite is a more informative parameter, since it measures actual removal under specified conditions. Variables such as ion selectivity, temperature, cation concentration, particle size, internal and external surface areas, pre-treatment of the zeolite and the presence of competing ions all affect the operating capacity. The cation exchange capacity of an ion exchange material reflects the capacity the material can remove when saturated with a highly preferred ion.

Direct comparison of exchange capacity between zeolites is difficult unless identical conditions are maintained. One method of comparison is to adopt a standard procedure and exchangeable ion. These conditions may not be optimal, and the maximum attainable exchange capacity may not be reached. The capacity will vary for each specific zeolite and cation, and will be strongly dependent upon environmental conditions.

Heavy metal adsorption capacity of a zeolite is defined as the mass of heavy metal ions taken up by a given quantity of zeolite at equilibrium. This is an important performance indicator and depends on a number of factors that include pretreatment, zeolite topology, solution pH, and temperature.

1.15) Kinetics

The three main stages that occur in ion exchange through zeolites are bulk diffusion through the solution, film diffusion through the boundary layer at the surface of the zeolite particle and particle diffusion through the matrix. The two rate controlling steps are film diffusion and particle diffusion, and the properties of the boundary layer and zeolite matrix are also clearly critical parameters. Reaction kinetics can be modelled based on the knowledge of concentration and activity gradients.

The relative rates of diffusion of the ions is also important, since the speeds of the incoming and outgoing ions within the zeolite may not be equal, causing a potential gradient to form, particularly if a

divalent ion is exchanging with a monovalent one, which may impede the faster species and accelerate the slower.

Chapter -2) Heavy metals and water treatment

2.1) Introduction to heavy metals

Heavy metal is a collective term applied to a group of metals and metalloids with density greater than 5 g/cm, and include elements such as Cu, Cd, Cr, Hg, As, Mn and Pb. Sources of heavy metals in the environment can be a vast variety of anthropogenic (man-made), as well as natural geochemical processes. Anthropogenic sources can be divided into point and diffuse sources. Point sources include mining and processing operations, industrial processes and waste disposal sites. These emissions can be controlled through legislation and regulation. Diffuse sources of heavy metal pollution include the combustion of fossil fuels, transportation, waste incineration, agricultural practices such as fertilizer, corrosion of metals and the dumping of contaminating materials such as used batteries. A summary of some of the heavy metals and their effects on human health is reported in Table 2-1 (Nascimento, Soares et al. 2009, Fu and Wang 2011, Hegazy, Abdelmaksod et al. 2014).

Table 2-1 Effects of heavy metals on human health

Heavy metal		**Effect**	**Permissible level (mg/L)**
Arsenic	As	Bronchitis, dermatitis, poisoning	0.01
Cadmium	Cd	Bronchitis, bone defects, increased blood pressure, kidney damage, Renal dysfunction	0.06
Chromium	Cr	nervous system damage, fatigue, irritability	0.05
Copper	Cu	liver and kidney damage, stomach and intestinal irritation, Anemia,	0.015
Lead	Pb	fatal infant encephalopathy, congenital paralysis, sensor neural deafness, liver, kidney, and gastrointestinal damage, nervous system damage	0.015
Manganese	Mn	damage to nervous central system	0.26

Mercury	Hg	protoplasm poisoning, spontaneous abortion, minor physiological changes, tremors, gingivitis, acrodynia	0.01

The toxicity of heavy metals depends on several factors including the dose, route of exposure, chemical species, as well as the age, gender, genetics, and nutritional status of exposed person. These systemic toxicants are known to induce multiple organ damages, even at low exposure levels (Barakat 2008, Yadanaparthi, Graybill et al. 2009, Barakat 2011).

The solubility of the metal governs its bio-availability, since the metal ion must reach a certain target molecule to have toxic effects. Toxic effects can be classified as chronic or acute. Chronic toxic effect occurs gradually, over time while acute toxins will cause an effect within a short period of time. One of the most common causes of heavy metal toxicity is their ability to impair normal enzyme activity in both humans and animals. A metal is considered most toxic if its effects occur so rapidly that medical treatment cannot be administered, or brain functions are affected. When the rate of uptake is greater than the rate of excretion, bioaccumulation occurs, and results in a gradual increase in heavy metal concentrations (Gupta and Ali 2004, Hui, Chao et al. 2005, Mishra and Patel 2009, Qiu and Zheng 2009, Barakat 2011, Belviso, Cavalcante et al. 2014).

2.2) Chemistry of Lead (Pb^{2+})

The chemical symbol for lead, Pb, is short for the Latin word plumbum, meaning liquid silver. Pb is a member of group 14 (IVA) of periodic table with atomic number of 82 and atomic weight of 207.18. It has a very high density (11.34 $g.cm^{-3}$) and a low melting point (327°C). Lead is a naturally occurring heavy metal that can be found in earth's crust and biosphere. Lead is not stable in its elemental state, but forms compounds in Pb (II) and Pb (IV) oxidation states. Pb (IV) forms a few compounds which are fairly stable due to complexation in water while Pb (II) is the most stable form of lead that has a high tendency to form basic salts with limited water solubility. in basic lead salts, OH^- anions partially replaces

other anions. Dissolution of lead in surface water depends on pH, temperature and the concentration of anions in water (Godwin 2001, Sublet, Simonnot et al. 2003, Mishra and Patel 2009).

2.2.1) Lead in Environment

Sources of lead in environment are natural and anthropogenic. Natural sources include weathering, volcanoes and dust. Anthropogenic activities, including mining and smelting of ore, combustion of coal and oil, waste incineration and manufacture of lead-containing products, are considered the primary source of lead in environment. Because of its exceptional properties, human exposure to lead is quite common. Typical concentrations of lead in wastewater from a tailing pond range from 0.5 to 25 mg/L. One third of the total estimated world's reserve of lead is located in North America (Agency for Toxic Substance and Disease Registry, 2005). Sources of lead in the home include lead plumbing and old paint, since lead was traditionally used as a paint pigment. Dust often contains high lead levels, particularly in urban areas where lead concentrations can be in excess of 100 mg/l. Aerial transport of these contaminated particles and subsequent deposition leads to crop contamination. Other sources of lead pollution include pesticides, metal processing and lead-acid batteries.

2.2.2) Health Effects of Lead

Breathing air, drinking water, eating food, or swallowing dust may expose people to lead compounds. Lead can cause neurological disorders particularly in children where mental development can be impaired. The most sensitive targets for lead toxicity are the developing nervous system, kidneys, hematological and cardiovascular systems. Common symptoms of lead poisoning include insomnia, loss of appetite, irascibility, weight loss, leading to eventual starvation. The rate of nerve impulses is reduced, and nerve damage and destruction can occur. Lead hinders the binding of oxygen by hemoglobin, and the substitution of zinc rather than iron when lead is present into porphyrin can result in anaemia due to Fe-porphyrin deficiency. At low exposure levels, lead affects mental and physical growth of children.

Considering cost, benefits and the ability of public water systems to detect and remove contaminants, US Environmental protection Agency (EPA) sets enforceable regulations called Maximum Contaminant Level (MCL). However, because lead contamination of drinking water often results from corrosion of the plumbing materials, for lead, a treatment technique is established rather than an MCL. The treatment technique regulation for lead is based on control of corrosivity of water. If lead concentrations exceeds an action level of 15 ppb in more than 10% of customer taps sampled, the system must undertake a number of additional actions to control corrosion. The public health goal for the concentration of lead in drinking water was set equal to zero in the national primary drinking water standard (2003). USEPA has also set pretreatment standards for some industrial effluents before discharging into a municipal wastewater treatment plant.

2.2.3) Lead Removal Methods

Different lead removal methods, including chemical precipitation, ion exchange, adsorption, electrodialysis, electrode deposition, filtration, Reverse Osmosis (RO) and evaporation recovery have been developed. For the removal of high concentrations of lead from wastewater, chemical precipitation processes are the most widely used methods.

The traditional method of heavy metal removal is by chemical precipitation. The aim of precipitation techniques is to convert a soluble contaminant metal ion into an insoluble form (such as a metal hydroxide) by chemical reaction, which can then be separated out and disposed of appropriately as a sludge. Several types of precipitation exist, depending on which chemical is added to transform the contaminant into an insoluble state. Ultimately, removal levels will depend upon the effectiveness of the separation of the solid phase so the type and density of precipitate is critical.

Hydroxide precipitation is the most common method used, as it is a Simple process that is easily automated and relatively low cost. Common precipitants are lime and caustic soda, both cheap and readily available. Many of the metal hydroxides are amphoteric, and soluble under high pH conditions, which

means that a careful control of pH is required. Hydroxide precipitates are colloidal, producing a low-density sludge with poor filtration characteristics, which is difficult to dewater. Pre-treatment with a reducing agent such as sodium metabisulfite may also be required if hexavalent chromium is to be precipitated. Hydroxide precipitation may be inhibited if complexing agents are present in the waste stream.

Sulfide precipitation method produces an insoluble metal sulfide, using either a soluble sulfide source such as sodium sulfide, or an insoluble source such as ferrous sulfide. The advantages of sulfide precipitation are that the process can operate under more acidic conditions (pH 2.0). Salts with lowest solubility products generally precipitate at lowest pH's. Sulfides also have higher reactivity, therefore reaction kinetic are faster and short contact times are expected.

Sulfide precipitates are not amphoteric and thus the process is not as pH dependent as hydroxide precipitation. Sulfide precipitation is, however, expensive compared to hydroxides, and there is a risk of generating hydrogen sulfide gas. Additionally, sulfides themselves may be toxic.

Carbonate precipitation produces a denser precipitate than hydroxides, under acidic conditions. The resulting sludge settles more easily, and is denser. Sodium bicarbonate has the advantages of being easy to handle, economic and available.

Co-precipitation is the effect when an otherwise soluble metal species is precipitated along with an insoluble precipitate. This can be due to adsorption onto the surface of the precipitate, the substitution of an ion from solution for one in the solid or the physical imprisonment of a small volume of solution within the precipitate pores. Adsorption is determined by factors such as the nature of the insoluble precipitate, the presence of complexing ligands and competing ions, solution pH and contact time. Alternatively, coprecipitation may occur due to composition of the wastewater, resulting in removals in excess of those that would be theoretically predicted for precipitation alone.

Precipitation is an economical technique but has a number of limitations:

• Relatively high chemical consumption, e.g. lime, soda ash

• Large sludge volumes are generated, which still require safe disposal

• There is no potential for recovery and reuse of the metals

• In a mixed waste stream no single pH will give maximum precipitation for all the metals present, and a compromise will have to be made with poorer removal performance for some if not all the metals. An alternative would be to have a multi-stage precipitation process, but this would reduce the simplicity of the treatment technique as well as increasing chemical consumption and sludge production.

• Variable waste streams, both in terms of composition and volume, can be difficult to treat using precipitation techniques, particularly in continuous processes.

• It is difficult to treat dilute wastewaters such as plating rinse waters by precipitation. It is also difficult to reach stringent effluent standards using this techniques.

Biological Treatment

Traditional biological treatment processes can tolerate some heavy metal content in raw effluent feeds, but severe declines in operational performance can be seen after critical concentrations are reached. Generally, biological treatment is not used for heavy metal effluents, particularly those with high or variable metal content, since shock loadings can prove toxic to the biomass.

Novel Methods

Although precipitation is the most common form of heavy metal removal adopted, there are a range of more sophisticated techniques that can be used. Adsorption, ion exchange, electrolytic recovery, biosorption, membrane processes, complexation, foam flotation and oxidation catalysis are just some of the new techniques that are now in use or under development. These techniques offer greater removal

efficiencies often linked with the opportunity to recover and reuse the heavy metals. Disadvantages may include significant capital or maintenance costs and the need for considerable operator input and knowledge

Electrolytic Recovery

Electrochemical technologies can be applied to metal-contaminated effluents with success. An electrical potential is applied to the effluent, and then depending on the charge of the metal ion, the ion will be attracted to either the anode or cathode. Similar removals to precipitation can be achieved, but this technology is not particularly appropriate for dilute waste streams. high potentials and long contact times are required, which can prove costly.

Biosorption

Many micro-organisms show significant sorption potential for heavy metal ions. The actual removal mechanism is either adsorption or ion exchange. depending upon the type of sorbent material. Living microbes can be used, but they can be subject to toxicity at high loadings and require nutrient supplements. Using dead microbes (biomass) has the advantage of still showing sorption potential.

Membrane Processes

Membrane processes consist of semi-permeable membranes of molecular dimensions, which permit molecules of certain sizes through, but exclude others. Types of membrane processes vary depending upon the pore size of the membrane used and the pressure applied to drive the effluent through the system. Ultrafiltration operates under gravity or a low pressure below 8 bar, with relatively large pores of about 20 Å. Reverse osmosis operates at higher pressure of about 30 bar, but has smaller pores (approximately 3 Å). The advantages of membrane technologies are their capability of producing very low residuals and their potential for reuse of the heavy metals, but the processes are quite sophisticated and require specialist operation. Membrane fouling is common, so pretreatment stages are usually

required. Membranes may also be unstable in some chemical environments, particularly in the presence of strong oxidizing agents and solvents.

Ion exchange and RO are both effective in producing a low concentration effluent but they have high operation and maintenance costs.

Adsorption method is generally preferred for removing Pb^{2+} ions due to its high efficiency, ease of handling, availability of different adsorbents and cost effectiveness. However, the use of commercial activated carbon is not an economical solution for wastewater treatment processes. Therefore, developing a low-cost and effective adsorbent material is crucial for lead removal from wastewater.

2.3) Adsorption

2.3.1) Mechanism of adsorption

Adsorption is the process of concentrating substances from solution onto a solid surface. The substance that is being removed from the liquid phase is called adsorbate while the adsorbent is the solid, liquid or gas phase that the adsorbate accumulates on it. Three types of bonding between the adsorbent material and adsorbate are characterized within environmental systems:

- Physisorption, also called physical adsorption, is a process in which the electronic structure of the species is barely perturbed upon adsorption. The bonds are weak and therefore physisorption is easily reversible.
- Chemisorption: Strong localized chemical bonds are formed between the adsorbate and adsorbent at active centers on the adsorbent. This process is largely irreversible except under extreme conditions.
- Electrostatic adsorption: Ions of one substance concentrate at interface as a result of electrostatic attraction to charged surface sites. Since this process is diffusion-controlled and electrostatic in nature, it occurs rather quickly.

Characterization of an adsorption process requires the study of the equilibrium distribution of the involved species and the rate the equilibrium condition is achieved. Activation energy is the most significant parameter governing rate of adsorption. Theoretical adsorption rate and adsorption equilibrium conditions can be identified in batch adsorption experiments.

Adsorption isotherms can be constructed by determining the uptake of adsorbate by specific adsorbents under constant temperature and applying a model to the data. This can be done either by varying adsorbent dosage or adsorbate concentration. Several models are available, with the most common being the Langmuir isotherm, the Freundlich isotherm and the Braun-Emmett-Teller (BET). If a linear relationship is obtained when the experimental data is plotted according to a specific isotherm, it can be assumed that the adsorbent concerned behaves according to the assumptions and suppositions made within that model.

Common practice when selecting an adsorbent to treat a specific waste stream is to perform a bench-scale study and fit the Langmuir and Freundlich isotherms to the experimental data to determine which model best describes the adsorbate removal. The appropriate isotherm relationship can then be used to calculate the maximum adsorption capacity of the material or predict the amount of adsorbate removed for a given adsorbent dosage. This information can then be considered during process design, or can provide a comparison between different adsorbents.

2.3.2) Activation energy of adsorption

The minimum amount of energy that is required to activate atoms or molecules to a condition in which they can undergo chemical transformation or physical transport is called activation energy (represented by symbol E_a). In transition-state theory, the activation energy is the difference in energy content between atoms or molecules in an activated or transition-state

configuration and the corresponding atoms and molecules in their initial configuration. Reactions with greater activation energy proceed slower. Since a plot of ln(k) versus 1/T will give a straight line with slope of E_a/R, activation energy can be directly calculated from rate constant at two or more different temperatures by using the following equation:

$$\ln\left(\frac{k_2}{k_1}\right) = \frac{E_a}{R}\left(\frac{T_2 - T_1}{T_2.T_1}\right) \qquad \text{Equation 2-1}$$

Where R= ideal gas constant (8.314 $J.K^{-1}.mol^{-1}$), E_a = activation energy ($J.mol^{-1}$), k_2 and k_1 are rate constants at absolute temperature T_1 and T_2, respectively.

2.3.3) Adsorption thermodynamics

The Gibbs free energy, enthalpy and entropy are the three fundamental thermodynamic functions of adsorption system, and are useful for assessing the overall heat and energies associated with adsorption processes. The Gibbs free energy is the energy available for a reaction at any particular state that reaches a value of zero at equilibrium state. If the Gibbs free energy change of an adsorption process from a non-equilibrium state to an equilibrium state at constant pressure and temperature is negative ($\Delta G° < 0$), this adsorption process occurs spontaneously. The value of the Gibbs free energy change in a standard state can be calculated as follows:

$$\Delta G° = -RT\ln K \qquad \text{Equation 2-2}$$

Where $\Delta G°$= changes in Gibbs free energy at standard state ($KJ.mol^{-1}$) and K= distribution coefficient which is calculated at different temperatures using the following equation:

$K = q_e/C_e$ Equation 2-3

The other two fundamental thermodynamic functions, the enthalpy change ($\Delta H°$) and the entropy change ($\Delta S°$) can be obtained from the slope and intercept of the plot of K against 1/T, using the following equation:

$\ln K = \Delta S°/R - \Delta H°/RT$ Equation 2-4

2.4) Rationale for using fly ash-based zeolites

Fly ash-based zeolites are characterized by a high cation exchange capacity and a high surface area. These properties and the availability of fly ash make it an economical and effective precursor for synthesis of adsorbent for heavy metal removal from wastewater. Therefore, this study was performed to study the synthesis of different types of zeolites from fly ash and investigate the effectiveness of synthesis products for the removal of lead ions from aqueous solutions.

This thesis will explore the feasibility of a sustainable, low cost, high-performance technology used in water treatment, geared specifically towards industries that require treatment of controlled or uncontrolled discharges of waste. The goal of this study is to develop an innovative material and method with significant commercial potential for removing heavy metals and organic contaminants from water. This will include investigation of optimized, low-cost processes for the production of a class of fine chemicals from industrial coal burning by-product. Characterization of the mineral, textural, morphological, and chemical properties of thus obtained zeolite products and improve operating parameters for efficient removal of heavy metal ions is another part of this study. Heavy metal-contaminated synthetic wastewater will be tested in batch adsorption experiments in contact with three types of fly ash-based synthetic zeolites (SOD, LTA, and Na-X). process parameters will be investigated to produce highly efficient adsorbents with high thermal and chemical stability. This study will include investigation of regenerative properties of the adsorbents suitable for treatment of large amounts of heavy

metal-contaminated water and the possibility of incorporation of the proposed materials into point-of-use devices will be analyzed.

2.5) Objectives of this work

- Develop suitable techniques to synthesize zeolitic adsorbents from fly ash for the removal of lead from wastewater.
- Characterize the morphology, crystallinity, surface, and stability of the synthetic zeolites.
- Optimize synthesis variables to achieve excellent adsorption for Pb^{2+} from wastewater
- Investigate adsorption behavior and suitability of known adsorption isotherms and kinetic models
- Determination of the thermal stability and water elution
- Pore size modification to obtain tailored crystal architecture

For this purpose, following zeolites were synthesized and characterized using different techniques. The main reason for the selection of this zeolites was the low Si/Al ratio and higher ratio of extra-framework cations suitable for ion exchange.

- SOD
- Na-X

2.6) Scope

The scope of this thesis includes the following tasks:

Review of the applicable techniques for the removal of heavy metal ions from water and investigate state of the art in the synthesis of zeolites

Synthesis and characterization of SOD and Na-X zeolites

Design of experiments to study the effects of pH, adsorbent dosage, and initial concentration of solution on lead adsorption capacity

Kinetic and isotherm studies

Investigation of regenerative properties of the adsorbents

Silver exchange studies to improve pore architecture and introduce antibacterial activity

Chapter -3) Experimental materials and methods

This chapter will explain the details of the experimental procedure, materials used and the methods developed throughout this study. Characterization methods are also discussed in more details in this chapter.

3.1) Fly ash

The fly ash sample was received from WE Energy Power Plant located in Oak Creek, USA and was used for the synthesis of SOD and Na-X zeolites. The received Fly ash was characterized and used as a precursor and source of silicon for zeolitic blend synthesis.

The chemical composition and the surface characteristics of the fly ash strongly depends on the type of coal, burning process and type of furnace. The following procedure was adopted to prepare fly ash samples. 8.0 g of the fly ash sample was subject to high-energy ball milling for 2.0 h. The samples were then passed through a standard No. 325 test sieve followed by drying in a vacuum oven at 90°C for 4 h. The sample was noted as FA. A scanning electron microscopy image of the FA is presented in *Figure 3-1*.

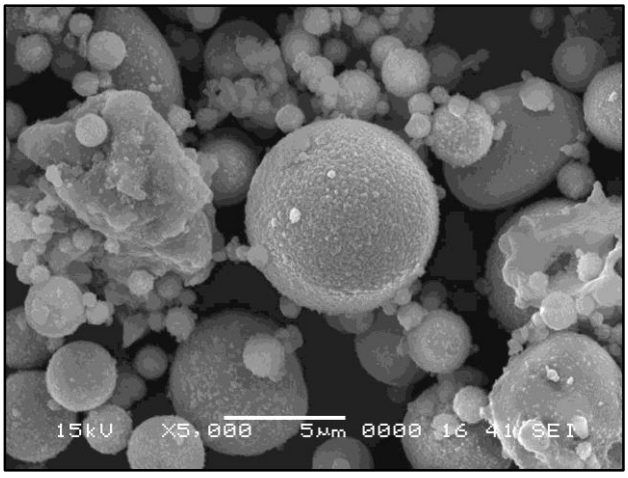

Figure 3-1 SEM image of FA, 5000X magnification

3.2) Chemicals

Water with a resistivity of 18.2 MΩ was used as Deionized (DI) water. All chemical reagents used within this study were analytical grade to minimize contamination.

There are two main methods for the synthesis of zeolites using solid waste that are recognized as one step and two step methods. The whole silica and alumina content of the ash is dissolved in alkali solution and recrystallized into zeolites that cover undissolved solid in the one step process. Morphological irregularities and variety of crystal types obtained are the major drawbacks of this method. The two step method requires separation of undissolved solid residue which tends to increase purity and reduces morphological irregularity. The drawbacks of this method are its low yield and a new solid waste left behind. Influencing variables, which affect the formation of a specific zeolite phase, are batch composition, Si/Al ratio and source of elements, alkalinity, water content, inorganic cations, presence of templates, solvent, temperature, aging, stirring and seeding.

3.3) One step method: Synthesis of hydroxy sodalite (SOD)

Due to its small aperture size, hydroxy sodalite is one of the most interesting sodalite family members, and an ideal candidate for the separation of small molecules and ions from aquatic mixtures. Hydrothermal activation process was employed to synthesize hydroxyl sodalite hydrate ($Na_8[AlSiO_4]_6(OH)_2.2H_2O$).

A 3M NaOH solution was used in the hydrothermal treatment of fly ash. The ratio of FA to alkaline solution was 30.0 g/200ml. The mixture was agitated with a mechanical mixer at 300 rpm. The extraction and precipitation of silicon content of fly ash was conducted in a 500 ml flask with reflux condenser under stirring for 24 hours at 348K. The treated sample was recovered by vacuum filtration and washed with DI water until pH reached below 9.0. The product was then dried in a vacuum oven at 363K, passed

through a No. 325 test sieve, stored in a desiccator to prevent contact with moisture, and was noted as ZCFA.

All chemicals used in the adsorption experiments were analytical grade, and a stock lead ion solution (1000 mg/dm^3) was prepared from analytical-grade lead nitrate (Aldrich Chemicals) which was dissolved in distilled water and serially diluted to working solutions of varying initial concentration for experimental purposes. $Pb(NO_3)_2$ was selected because it is readily soluble in water. 0.1N HCl or NaOH was used to adjust the pH of the initial heavy metal solution to 5.5.

3.4) Two step method: Synthesis of Na-X zeolite

A two-step method was employed to transform FA into Na-X zeolite. Silica was extracted from FA in a fusion extraction process performed on a mixture of NaOH and FA. Equal weights of FA and NaOH were heated at 800K in a box furnace for 1.0 hr. The fused mass was cooled down to room temperature followed by milling with an SPEX ball mill for 120 minutes. Each gram of the fused powder was mixed with 5.0 mL DI water and agitated at room temperature for 4.0 hrs. at 300 rpm. The solid residue was then filtered out and the concentration of silicon was determined. 2 M solution of sodium aluminate ($NaAlO_2$) was mixed with the supernatant for preparing reaction mixture with predetermined Si/Al molar ratio. The reaction mixture was agitated for 1.0 hr. followed by hydrothermal treatment in different temperatures inside a Teflon lined acid digestion vessel (Parr Instruments). Washing the precipitates with DI water until pH reached a value of 8.0, treatment with 2M NaCl solution to exchange alkali and alkaline earth atoms with sodium, separation of sodium exchanged zeolite using 0.45 µm filter paper, and drying in a vacuum oven at 370K were the final steps of the process.

3.5) Analytical techniques

The following techniques were used to characterize the samples:

3.5.1) X-ray Diffraction

Since zeolite materials are crystalline solids, they have a characteristic diffraction pattern that can be used to identify their exact structure and to determine their degree of crystallinity. The diffractions of X-rays from zeolite crystallites produce a scattering pattern which is specific of the arrangement of arrays of atoms or ions located within the zeolite structure. Each zeolite has its own specific pattern. This technique can also show whether the solid sample is amorphous or crystalline phase. The purity of the solid crystal will be measured by comparison of the X-ray pattern of the sample with X-ray pattern of the standard sample.

The principal equation used in the analysis of X-ray powder patterns is the Bragg law which states that:

$n\lambda=2d_{hkl}.Sin\theta_{hkl}$ Equation 3-1

Where n is the order of diffraction (1, 2,…), λ is the wavelength of the X-ray beam. θ_{hkl} is the Bragg angle between the incident X-ray beam and the crystal planes and d_{hkl} is the inter-planar distance on a set of planes. A schematic diagram of X-ray diffraction of a crystal is presented in Figure 3-2

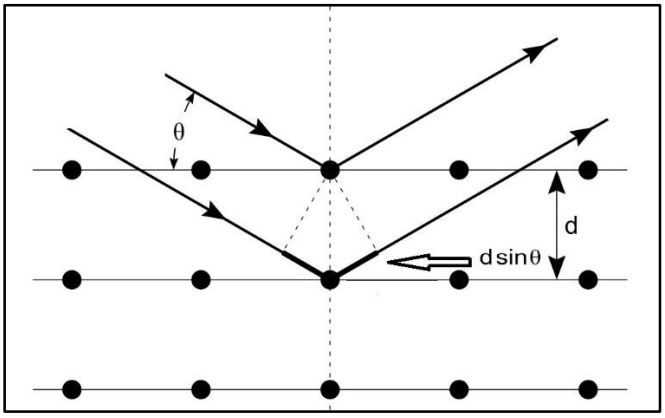

Figure 3-2 Diffraction of X-rays by a crystal

In the diffractometer, the intensity of the diffracted beam is measured directly by an electronic counter that counts the number of pulses per unit time. This number is directly proportional to the intensity of the

diffracted X-ray beam that enters the counter. A monochromatic (filtered) radiation is used in the diffractometer, and the X-ray detector is placed on the circumference of a circle centered on the powdered sample. 1.5 g of the samples with particle size below 10 μm was packed into an XRD sample holder. XRD pattern was obtained using an Advanced D8 Discover Bruker diffractometer which is shown in Figure 3. By scanning over the angle range from 5-60° 2θ at 0.2°/min in the step mode. The detector was LYNXEYE-XE and the analysis was operated at 40.0 kV and 40.0 mA (Cu-Kα1 =1.5406 Å). The sums of intensities of six strong peaks in the range of 11-32° 2θ was used in the calculation of percent crystallinity. The identification of the phases present was done using EVA crystallographic software equipped with "International Center for Diffraction Data Powder Diffraction File" database (ICDD-PDF 2.0). All measurements of the finely ground powder samples were taken at room temperature.

Figure 3-3 XRD instrument (Bruker- D8 Discover)

3.5.2) Scanning Electron Microscopy and Energy Dispersive Spectroscopy

Scanning electron microscope (SEM) is a very helpful technique to investigate the fine details of the interior structure of specimens in high magnifications. The size and morphology of the adsorbent crystals were examined at several different magnifications using a JEOL JSM-6460 LV electron microscope. The

obtained micrographs have a similar appearance to traditional optical microscopes. In contrast to optical microscopes, SEM is capable of achieving magnification as high as 80,000X, which make it the perfect tool to analyze and study the surface of samples. This technique provide topographical, compositional and crystallographic information.

SEM uses a focused beam of electrons. The interaction of the electron beam gives secondary electrons, backscattered electrons, Auger electrons, characteristic X-rays, and photons of various energies. The backscattered and secondary electrons can be observed by their respective detectors, and are used for imaging. The secondary electrons are mainly used to form topographic images of the surface.

Energy Dispersive X-ray spectroscopy (EDX) is an analytical tool, usually attached to the SEM for measurement of the surface elemental composition (typical depth is ~10µm). The incident beam excites electrons in inner shell, prompting their ejection. An electron from the outer, higher energy shell of atom fills the gap, therefore the excess energy of the electron is released in the form of an X-ray. The released X-ray creates spectral lines that are highly specific to individual elements.

Figure 3-4 SEM-EDX instrument (JEOL JSM-6460)

3.5.3) Textural analysis

In order to optimize the application of microporous and mesoporous materials, an accurate textural characterization is crucial. Total surface area determines accessibility of active sites and pore architecture (pore size, size distribution, and pore volume) controls selectivity and transport phenomena. Gas adsorption is among the most popular experimental methods for characterization of porous materials. The shape and type of adsorption isotherms are governed by atomic interactions, available pore space and thermodynamic stability of fluid in narrow pores.

It is necessary to remove all physically bound fluid from the adsorbent surface in order to obtain correct and reproducible results. This can be accomplished by purging with an inert gas or vacuum pumping at elevated temperatures. Degassing under vacuum condition is especially important for zeolite adsorbents because the adsorption measurement often start at very low pressure below 0.01 Pa. A turbo-molecular pump coupled with a diaphragm roughing pump allows the physisorbed water to be removed. Water, when adsorbed in micropores (as expected in this study) is more persistent than the water adsorbed by mesoporous or nonporous materials and needs high temperature (up to 673K) and long outgassing period which requires a special heating program.

Nitrogen at 77K is considered to be the standard adsorptive for micropore and mesopore size analysis. Nitrogen adsorption experiments were carried out to investigate the textural properties using an ASAP 2020 Micromeritics specific surface analyzer. Determination of specific surface area was based on the shape of the nitrogen adsorption/desorption isotherms in 77K. The relative pressure range was 10^{-6} to 0.99. Before the measurements, the samples were degassed in two stages. Evacuation stage started with a temperature ramp rate of 10K/min to target temperature of 363K. Evacuation rate was set to 50 mmHg/s followed by unrestricted evacuation below 5.00 mmHg down to a vacuum set point of 500 μmHg in 120 min. The heating stage involved a 10K/min ramp to a target temperature of 673K. Hold time and pressure were 600 min and 20 mmHg respectively. The BET multilayer adsorption theory was employed in a

range of p/p_0 between 0.06 and 0.3 to determine S_{BET}. (p and p_0 are: equilibrium pressure and saturation pressure of nitrogen, respectively).

Figure 3-5 Specific surface analyzer (ASAP 2020 Micromeritics)

3.5.4) Cation Exchange Capacity (CEC)

Presence of loosely bound cations of alkali and alkaline earth elements, results in exchange capacity of zeolites. Cation exchange capacity (CEC) is an important characteristic of zeolites in adsorption application. CEC defines the concentration of negatively charged sites of the adsorbent that can adsorb exchangeable cations. The ammonium acetate saturation method involves the saturation of zeolite with a solution of ammonium acetate. Unlike Methylene Blue Absorption (MBA) method, Ammonium Acetate Saturation (AMAS) can be employed to measure the CEC of the zeolite products. Samples were washed to remove soluble phases. 1.0 gr of each sample was transferred to a centrifuge tube. 30 mL of 1.0 N solution of CH_3COONa was added. The mixture was centrifuged and the clear liquid was discarded. The saturation was repeated four times to ensure all cations in the zeolite are replaced with Na. The zeolite was washed with isopropanol to ensure the zeolite was clean. Then the dried zeolite was weighed and mixed with CH_3COONH_4 to replace Na with NH_4, this procedure was repeated twice. The liquid phase was decanted into a 100 mL flask after each successive centrifugation.

The concentration of Na, Ca and Mg in the supernatant was measured. The CEC values can be affected by homogeneity of the zeolite deposit. α-Quartz phase present in the original fly ash does not have a positive influence on the CEC (Rhoades 1982, Mondale, Carland et al. 1995, Kitsopoulos 1999).

3.5.5) pH measurement

The pH value of the solutions containing fly ash was measured using the following method: 0.5 gr of fly ash was added to 50 mL of deionized water (pH=7.0) and maintained at 25°C for 4 hours. The aqueous sample was taken and filtered by a filter paper. The solution pH was measured using a digital pH meter.

3.5.6) Stock and reference solutions

The glassware used in the experiments were first washed with Liqui-nox detergent and rinsed with water. Rinse with 10% nitric acid solution and DI water were performed to remove traces of contamination and then the glassware were dried at 330K.

Lead standard solution (1000 ppm) was obtained from Sigma-Aldrich. Working solutions with a lead concentration of ~10ppm concentration were prepared by dissolving 0.0159 g lead nitrate in 1000 mL DI water. The pH of the solution was adjusted by addition of 0.1N NaOH or HCl. 20.00 mg zeolite was added to 100 mL of lead solution in 125 mL Erlenmeyer flask and sealed with Parafilm. A control solution in the absence of zeolite was prepared to determine the adsorption of lead to the glassware.

3.6) Pb^{2+} adsorption using Sodalite

Solutions of Pb^{2+} with concentrations ranging from 0-500 mg/L were prepared from a stock of 1000 mg/L lead nitrate ($Pb(NO_3)_2$) solution stabilized with nitric acid (10% HNO_3). The optimal contact time was evaluated on suspensions of 250.0 mg sodalite (ZCFA) in 50 mL solutions of Pb^{2+}. The residual metal concentration in the supernatant was analyzed by AAS.

To investigate the adsorption isotherms and adsorption efficiency, the cation solutions were stirred up to 12 hours at room temperature. The substrate was separated and the supernatant was analyzed. The influence of process parameters, including contact time, adsorbent dosage and initial metal concentration, were investigated. The removal efficiency (η), was calculated according Equation below:

$$\eta = \frac{(C^{i}_{cation} - C^{e}_{cation}) \times 100}{C^{i}_{cation}} \qquad \text{Equation 3-2}$$

Where C^{i}_{cation} and C^{e}_{cation} are the initial and equilibrated concentrations of Pb^{2+} in solution (mg/L)

Distribution of the adsorbate species between the aqueous phase and adsorbent is described using adsorption isotherms, based on a set of assumptions about the type of coverage, possibility of interaction between the adsorbate species, and the uniformity (heterogeneity/homogeneity) of the adsorbent. Adsorption data describes the relationship between adsorption capacity and concentration of adsorbate at constant temperature. The selection of appropriate correlation models for the experimental equilibrium data is important in order to optimize the design of an adsorption system for the removal of Pb^{2+} from water. Langmuir and Freundlich isotherm models are shown to fit the equilibrium behavior of heavy metals adsorption processes. These two models were used to correlate the observed behavior in the present study.

3.7) Lead adsorption using Na-X

3.7.1) Batch kinetic studies

Kinetic studies were conducted to determine the equilibrium time for the adsorption of lead onto zeolite. 15 samples (Triplicate) were prepared for kinetic studies. The samples were shaken at 150 rpm using a laboratory shaker and withdrawn within 180 minutes. Filter paper (0.45 µm) was used for the separation of adsorbent from the liquid phase. The concentration of Pb (II) in the solutions was determined using a

Thermo Electron Corporation, S series Atomic Absorption Spectrometer (Figure 3-6). The detection limit of flame atomic absorption for Pb^2 with a characteristic λ of 217 nm was 10 µg/L.

Figure 3-6 Atomic absorption spectrometer

3.7.2) pH effect studies

The optimum acidity at which maximum adsorption of lead using zeolite would occur was determined by varying the pH of the stock solution between 3.0 to 6.0 in increments of 0.5 unit. 20.00 mg of zeolite was added to 100 mL of lead working solution. (initial concentration ~10 ppm). The mixture was shaken at 150 rpm at room temperature and the pH was recorded after 180 min. The sample was then filtered and the Pb^{2+} concentration in the filtrate was measured.

3.7.3) Isotherm studies

Eight different dosages of adsorbent (10.00 to 60.00 mg) were added to 250 mL of 10 ppm lead solution at pH values ranging from 3.0 to 6.0 and the mixture was shaken at 150 rpm. The lead concentration detection was carried out by flame atomic absorption spectrometry.

3.7.4) Desorption studies

Desorption studies were performed to investigate the leaching of adsorbed lead ions from zeolite. Eight different weights of zeolite in the range of 10.00 to 60.00 mg were added to 10 ppm lead solution and mixed at 150 rpm for 180 min. The zeolite was then recovered with centrifugation and added to 250 mL of DI water and stirred at 150 rpm for another 180 min. The liquid phase was subject to atomic absorption spectroscopy. A control study was also performed to determine lead ion content of the zeolite by adding representative weights of fresh zeolite into 250 mL of DI water.

Chapter -4) Results and discussions

4.1) Characterization of Fly ash

XRD method was used to analyze the crystalline phases of FA. The XRD diffraction pattern of the precursor of zeolite synthesis (FA) is presented in Figure 4-1. The presence of crystalline minerals Mullite ($Al_6Si_2O_{13}$), hematite, magnetite and lime with large characteristic quartz (SiO_2) peaks was detected.

The amount of crystalline material versus glassy aluminosilicate phase depends largely on the coal combustion process used at a particular power plant. When the maximum temperature of the combustion process is above approximately 1470K (specially with a high cooling rate), the ash produced is mostly glassy phase material while with a more gradual cooling rate, crystalline phases can grow. In general, factors affecting the mineralogy of coal fly ash are chemical composition of the coal, coal combustion process, and additives used (flame stabilizer and corrosion inhibitors). The mineralogy and crystallinity of fly ash is governed by boiler design while the presence of minerals in coal dictates its elemental composition. As can be seen in Figure 4-1, the major phases present in FA sample were Quartz, Mullite, Hematite, Magnetite, and Lime. X-ray diffractometric (XRD) results indicated the presence of aggregates composed of, α-quartz (SiO_2), Hematite and iron oxides in the fly ash.

The observation of fly ash particulates on the scale of micrometers was performed using scanning electron microscopy. Amorphous irregular forms and polycrystalline aggregates were observed in SEM micrographs of FA with the most abundant morphology being spherical with relatively smooth surface grain (Figure 4-1). Iron oxide in form of magnetic inclusion was seen on the outer surface of aluminosilicate spheres of FA.

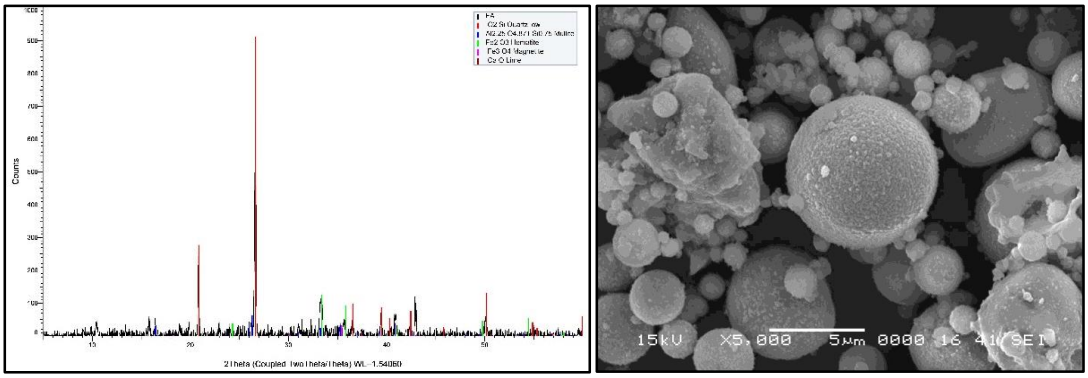

Figure 4-1 The XRD pattern and SEM micrographs of fly ash (left and right, respectively)

The major elements in the FA composition were C, O, Na, Mg, Si, Al, S, K, Ca, Fe and Ti. The elemental composition of the FA based on energy dispersive spectroscopy is presented in Table 4-1 Elemental composition of fly ash

Table 4-1 Elemental composition of fly ash

Element	**C**	**O**	**Na**	**Mg**	**Al**	**Si**	**S**	**K**	**Ca**	**Ti**	**Fe**
Atomic percent	51.79	30.41	0.62	1.05	3.38	6.48	0.15	0.19	4.56	0.23	1.13
Standard	$CaCO_3$	SiO_2	Albite	MgO	Al_2O_3	SiO_2	FeS_2	Feldspar	Wollastonite	Ti	Fe

4.2) Characterization of Na-X

The XRD pattern of the synthesized zeolites confirmed that following the zeolitization process, crystallization of silica and alumina occurred with a predominant formation of pure form high crystalline Na-X zeolite with space group Fd-3 which is classified as FAU (Faujasite). The crystal data of the obtained zeolite is presented in Table 4-2.

Table 4-2 Crystal data of Na-X zeolite

Name	Refined Composition	Space group	a	b	c	α	β	γ
Na-X hydrated	$Na_{88}Al_{88}Si_{104}O_{384}(H2O)_{172.1}$	Fd-3	2.503	2.503	2.503	90	90	90

Mullite and α-quartz peaks seen in XRD pattern of the FA sample disappeared and all major peaks correspond to Na-X zeolite structures. By analyzing the diffraction results, it can be stated that zeolite Na–X needs a long process time (>18 hr.) to be fully formed. Zeolite X has complex and large polymeric

silicate units. The average crystal size of the prepared zeolite was estimated by Scherrer's equation. Increasing the crystallization time from 8 to 48 hr., increased the average crystal size from 250 to 720 nm. However, it did not change the structure of the zeolite product. The crystallinity of the samples was calculated based on ASTM 3906 methodology. The results are presented in Table 4-4.

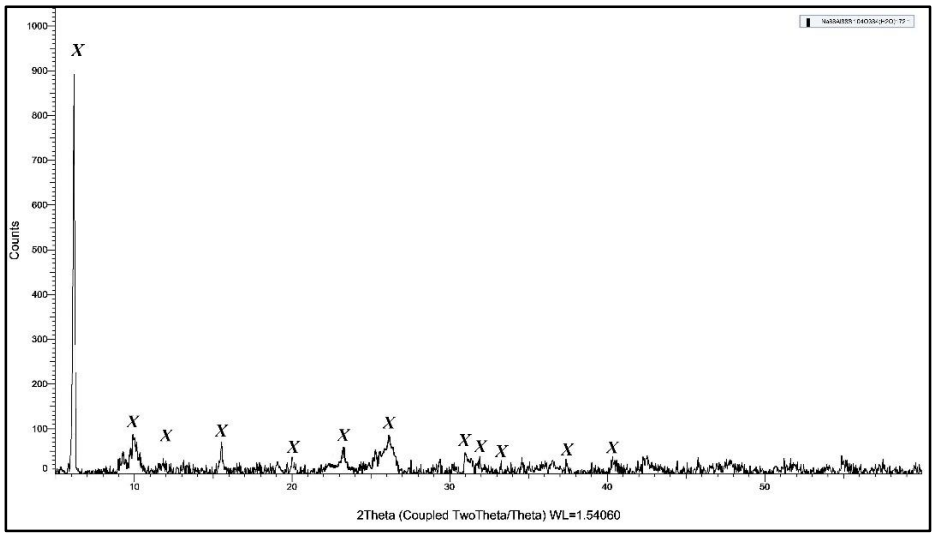

Figure 4-2 The XRD pattern of zeolite Na-X synthesized during 24 hr.

Morphological features of synthesized zeolites are presented in Figure 3. Scanning Electron Microscopy (SEM) provided evidence of growth of Na-X zeolite in 370K. Formation of crystals started after 2.0 hr. the spheres and agglomerates changed to crystal shapes stacked to form aggregates. The mechanism of zeolite synthesis involved three steps, namely dissolution, condensation and crystallization. Quantitative EDX analysis using spot size of 54, working distance of 10 mm and dead-time > 45% using Inca software package resulted in the identification of the elements listed in Table 4-3 in the zeolite product.

Table 4-3 Elemental composition of Na-X

Element	C	O	Na	Mg	Al	Si	Ca	Ti	Fe
Atomic percent	12.37	58.51	3.00	1.62	7.2	8.8	7.95	0.44	0.11
Standard	$CaCO_3$	SiO_2	Albite	MgO	Al_2O_3	SiO_2	Wollastonite	Ti	Fe

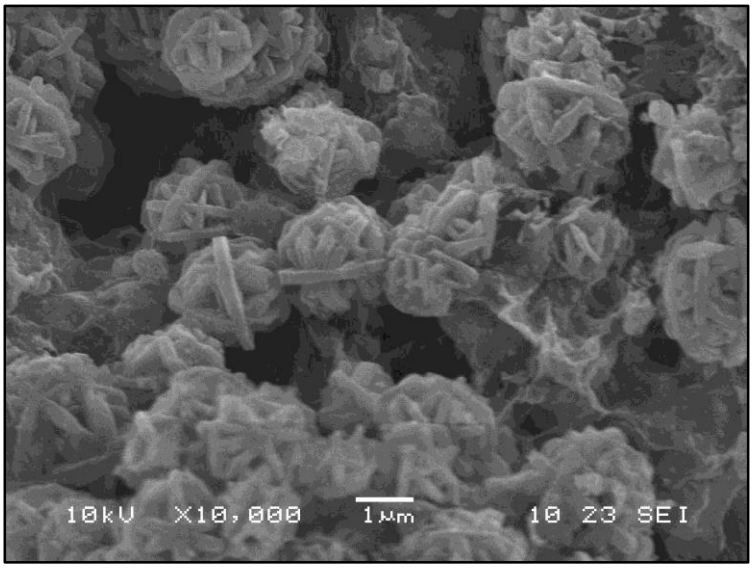

Figure 4-3 Na-X zeolite crystals formed after 18 hr. at 370K

4.2.1) Pore size analysis by physisorption method

In order to find the optimum crystallization time and the maximum specific surface area, the BET analysis were performed on samples with different crystallization time and results are presented in Table 4-4. Increasing crystallization time led to growth of larger crystals particles. One of the most important information obtained from a physisorption experiment about surface and porosity is the shape of isotherm, which reveals the kind of porosity of sample. Type I(a) isotherm are characteristic of microporous adsorbents. According to definition of Brunauer, the products are characterized by type I isotherms. The isotherm linear plot of the adsorption and desorption branches for the Na-X sample after 48 hr crystallization time is presented in Figure 4-4. The hysteresis loop seen in the multilayer range of isotherm is associated with the mesopore filling and can be due to contraction and slow expansion of the adsorbent.

Table 4-4 The specific surface area, crystallinity, pore width and pore volume of Na-X zeolite

Crystallization time (hr)	**BET surfaces area (m^2/g)**	**Crystallinity (%)**	**Adsorption average pore width (nm)**	**BJH desorption cumulative volume of pores (cm^3/g)**	**CEC (meq/100g)**
1	13	44	17.0	0.3362	170
4	117	69	12.8	0.3639	213
8	170	73	9.6	0.3833	374
24	409.2	79	5.6	0.3919	357
48	424.3	78	3.3	0.4271	378

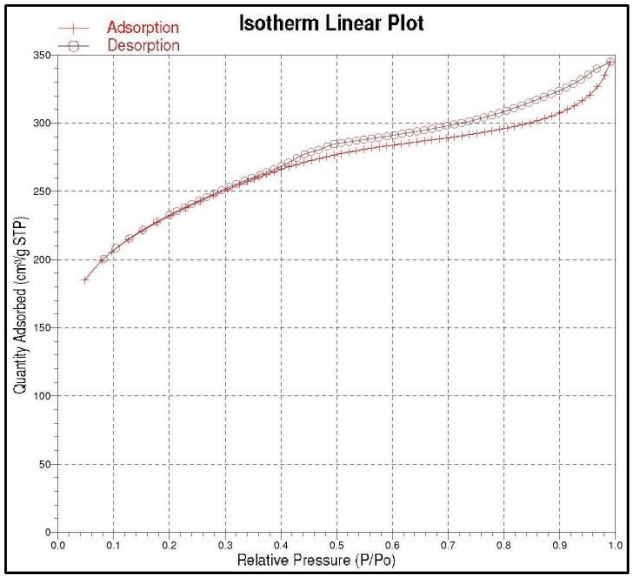

Figure 4-4 . Isotherm linear plot of Na-X zeolite after 48 hr crystallization

4.2.2) Thermal behavior

TG and DTA provide quantitative information on the dehydration and decomposition of guest molecules. The resulting TGA thermogram of hydrated Na-X zeolite indicated that the zeolite underwent two different water loss events. The first event happened due to evolution of weakly bound water (330-450K) located in the upper cages of the zeolite, and the second event (450-700K) could be related to the more water molecules bound more tightly inside the sodalite cages of the framework. An exothermic degradation peak was detected at 1230K that can corresponds to the collapse of zeolite structure.

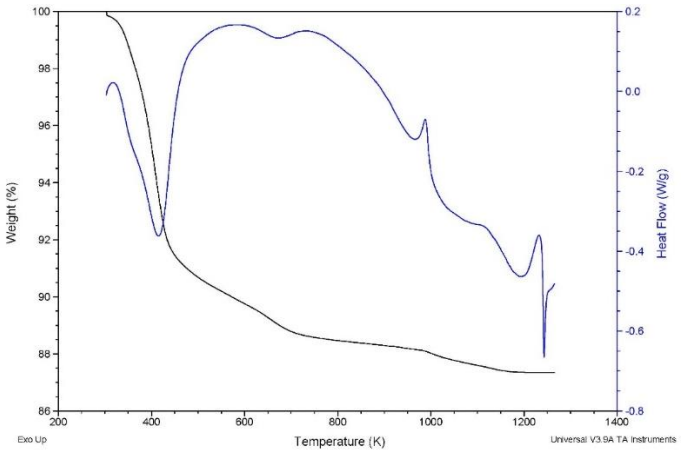

Figure 4-5 DTA curve of the Na-X zeolite illustrating thermal decomposition of NA-X

4.3) Characterization of SOD

4.3.1) XRD analysis

The XRD patterns of the fly ash (FA) and product of hydrothermal activation (ZCFA) are presented in Figure 4-6.

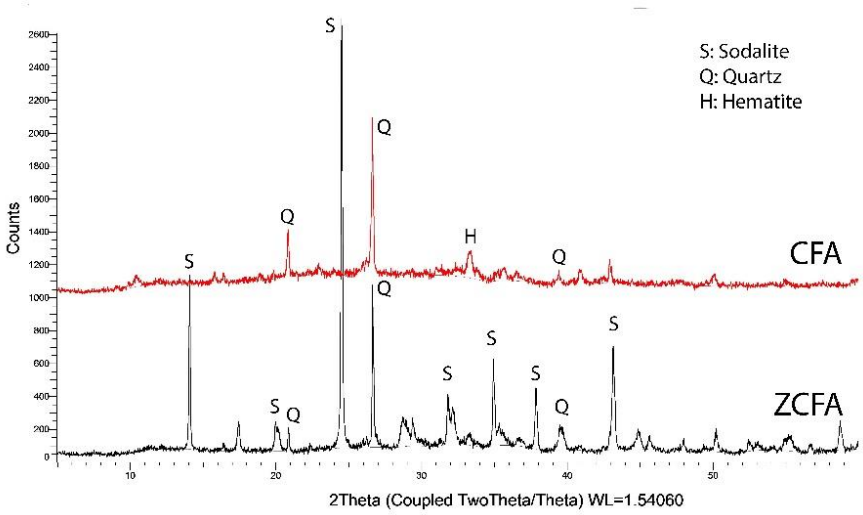

Figure 4-6 XRD patterns of CFA (upper) and sodalite (lower)

The XRD patterns show that some crystalline phases of CFA are mostly absent in the new material (ZCFA), and the new crystalline phase present in ZCFA are sodalite and α-quartz. Sodalite shows a framework with cubic symmetry constructed from vertex sharing of SiO_4 and AlO_4 into four and six-membered oxygen-rings, forming a cage structure known as β-cage. Owing to its framework flexibility, Sodalite can accommodate different anions such as hydroxy. Due to the small aperture size (2.7Å) of hydroxy sodalite ($Na_8[AlSiO_4]_6(OH)_2$), the material can also be an ideal candidate for the separation of small molecules such as H_2 (2.95Å) from gas mixtures.

4.3.2) SEM/EDX

The dominant morphological forms seen in electron micrographs of the FA were spheres of amorphous aluminosilicate glass. Most of these spheres occur individually but they also form intergrowth. Fly ash-

based Hydroxy sodalite forms sphere-like crystals that stack to form aggregates. SEM micrographs of the adsorbents are presented in Figure 4-7. The original fly ash particles typically were spherical in shape with an almost smooth surface made of an alumino-silicate glass phase and iron oxide inclusions. The other forms seen in SEM micrographs were amorphous aggregates at different sizes. Upon formation of the zeolite, the surface became rough, indicating the deposition of clusters of zeolite crystals.

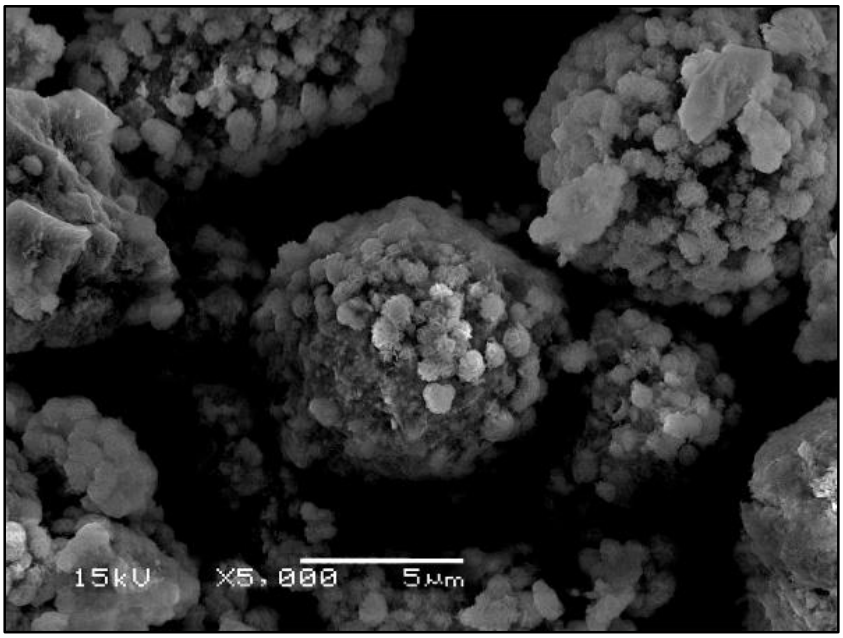

Figure 4-7SEM photomicrographs of sodalite sample at 5000X magnification showing the presence of clusters of crystallized zeolite

4.3.3) BET Surface area

Adsorption/desorption isotherm of nitrogen for fly ash represented type II and IV isotherm, which is characteristic of macroporous materials and corresponds to a situation when a monolayer of N_2 at low compressibility on the surface of the adsorbate is formed. Specific surface area is an important parameter in the application of adsorbents. As a result of zeolitization process, the BET surface area increased significantly because of the change in the texture of micropores in the zeolite structure. Higher BET surface results in a larger surface area of adsorbent exposed to the adsorbate and can lead to higher adsorption capacity. Type IV isotherm was applicable as revealed by nitrogen adsorption/desorption

isotherms (Figure 4-8). The hysteresis seen between the adsorption (lower) and desorption (upper) curves indicates mesoporosity (existence of pores in the range of 2-50 nm).

Table 4-5 BET surface area, t-plot micropore volume and t-plot micropore surface of ZCFA and CFA

Adsorbent	BET surface area (m^2/g)	Micropore volume (t-plot) (cm^3/g)	Micropore surface (m^2/g)	CEC (meq/100g)
CFA	13.87	0.00292	5.542	11
ZCFA	43.6	0.0048	9.62	320

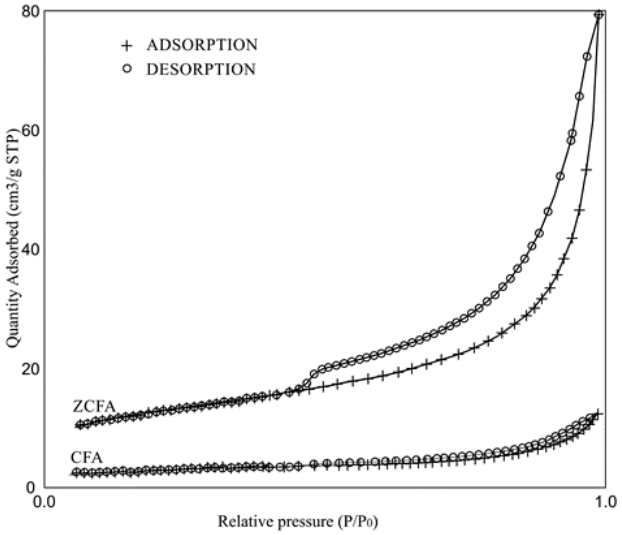

Figure 4-8 Nitrogen adsorption/desorption isotherm for ZCFA (Sodalite) and CFA (Fly ash)

4.3.4) Cation Exchange Capacity

The CEC of the ZCFA was 320 meq/100g which is 29 times higher than CEC of fly ash (11 meq/100g). Despite the satisfactory potential in ion exchange capacity of the fly ash by itself (Blissett and Rowson 2012, Shyam, Puri et al. 2013, Belviso, Cavalcante et al. 2014, Yao, Ji et al. 2015), product of its zeolitization showed significantly higher ion exchange capacity.

4.4) Lead adsorption using Na-X

4.4.1) Kinetic studies

In order to evaluate the effect of pH on equilibrium time, batch experiments were conducted at pH values of 3.0, 4.0, 5.0, and 6.0. Profile of Pb^{2+} removal efficiency versus agitation time is presented in Figure 4-9 The adsorption of lead on zeolite was conducted in three steps. The first step (within the first 10 minutes) was the fastest step, followed by an intermediate step where the rate of change in concentration was lower than the initial step and accounted for 25-30% of total adsorption capacity. Slight changes in concentration was detected during the slow final step. The equilibrium time is defined as the time in which system reaches a chemical equilibrium where the concentration of the product and the reactants cease to change with time. The equilibrium time in this study is defined as the minimum time after which, concentration of solute does not change more than 5% over time. The equilibrium time was found to be 150 min in pH ranging between 3 and 4 and 120 min at more neutral environment (pH 5 and 6).

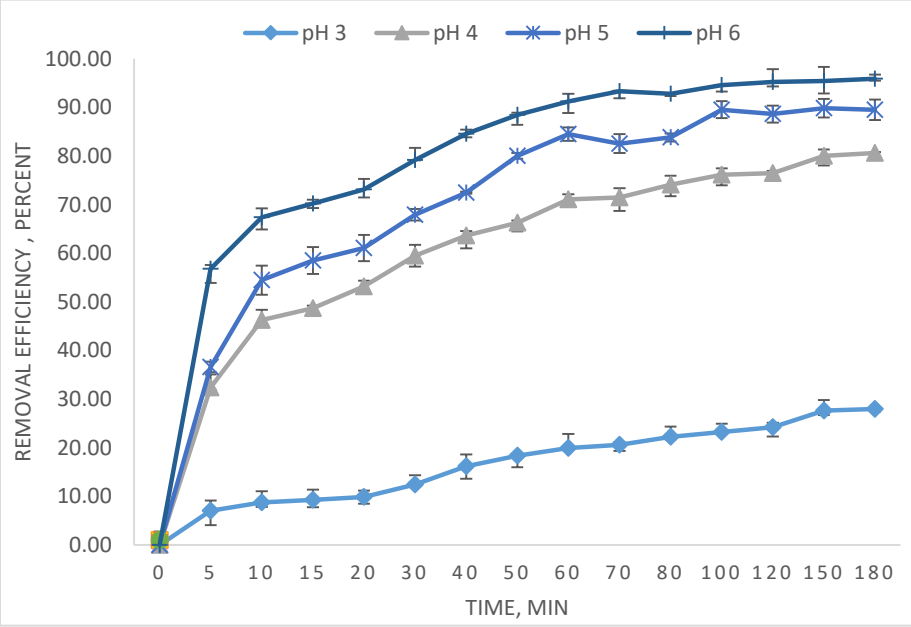

Figure 4-9 Lead removal efficiency of fly ash-based zeolite Na-X vs time at pH 3, 4, 5 and 6

Batch adsorption experiments were conducted at different pH values ranging from 3.0 to 6.0 by contacting zeolite with lead solution with initial concentration of approximately 10 mg/L. After three hours, the pH was measured and recorded. Metal ion's adsorption is affected by pH, properties of adsorbent, adsorbate, temperature, concentration and presence of competing ions in solution, among others. A sharp increase in adsorption efficiency was observed within a pH range of 3.0 to 4.0 and the best performance was detected in pH 6.0 while the removal efficiency was very poor in strongly acidic environment (pH=3) which can be due to instability of zeolite framework at lower pH values. At low pH, some functional groups may be positively charged and their interaction with metal ions can be hindered significantly. The graph of maximum lead removal efficiency of Na-X in different pH values is presented in Figure 4-11.

Batch adsorption experiments showed that Pb^{2+} can be effectively removed from aqueous solution using fly ash-based zeolite. The contact time necessary for maximum adsorption was found to be between 120-150 min at room temperature.

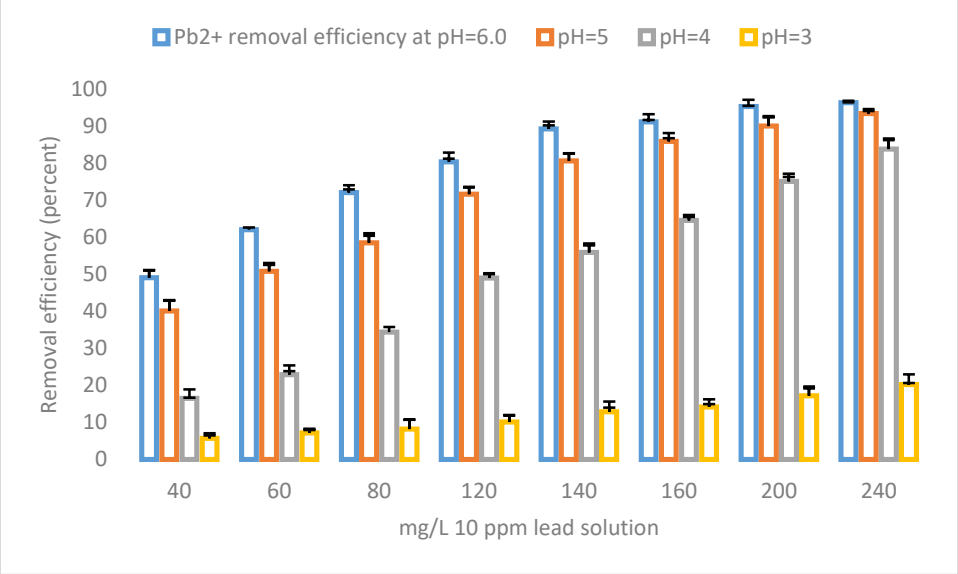

Figure 4-10 Lead removal efficiency vs adsorbent dosage at pH 3 to 6. Initial Pb^{2+} concentration: 10 ppm.

The pH level of the solutions was an important factor in the removal of lead. The reaction rate increased with increasing pH. Zeolite dosage was also an important parameter in effectiveness of adsorption process. As can be seen in Figure 4-10, The removal efficiency increased from 49% to 96% when the zeolite dosage was increased from 10 mg to 60 mg at pH value of 6.0. The disposal of zeolite after use needs to be properly considered.

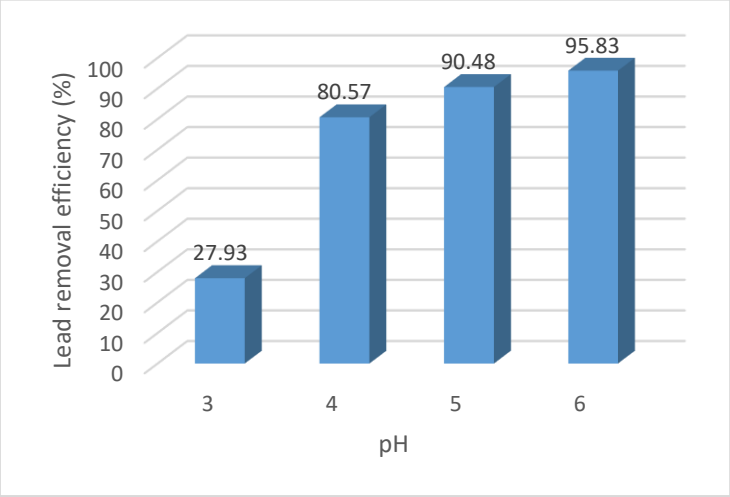

Figure 4-11 Maximum Lead removal using 0.6 gr/L fly ash-based Na-X at pH 3, 4, 5 and 6 (initial lead concentration is 10 ppm)

Adsorption kinetics analysis provides a valuable insight into the reaction pathway and the mechanisms involved and is one of the most important aspects of adsorption. A kinetic model developed from experimental data is able to predict the removal rate of a specific pollutant and therefore an appropriate system can be designed. Pseudo-first order (Lagergren) rate expression is a kinetic model that is generally adopted for adsorption analysis in the following form:

$$\frac{dq_t}{dt} = k_L(q_e - q_t) \qquad \text{Equation 4-1}$$

Where k_L= Lagergren rate constant, q_e=equilibrium adsorption of solute, and q_t=amount of solute adsorbed at time t.

Integration of above equation for boundary conditions t=0 to t=t and q_t=0 to q_t= q_t gives:

$$\ln(q_e - q_t) = \ln(q_e) - k_L t$$ Equation 4-2

The above equation can be rearranged to obtain the non-linear form where amount of adsorbed solute can be calculated over time:

$$q_t = q_e(1 - \exp(-k_L t))$$ Equation 4-3

Kinetics of adsorption can also be modeled using pseudo-second order equation (Ho's model) in the following form:

$$\frac{dq_t}{dt} = k_H(q_e - q_t)^2$$ Equation 4-4

Where k_H= adsorption rate constant ($g.mg^{-1}.h^{-1}$). Integration of above equation for the same boundary conditions as pseudo-first order model gives:

$$\frac{t}{q_t} = \frac{1}{k_H {q_e}^2} + \frac{1}{q_e} t$$ Equation 4-5

Where k_H is the second order reaction rate constant for adsorption.

The pseudo-first order reaction rate model and pseudo-second order reaction rate models were used to describe the kinetics of lead adsorption onto zeolite. The batch kinetic adsorption data were fitted to the mentioned models by non-linear regression analysis. It can be observed that the pseudo second order model better described the adsorption of Pb^{2+} on Na-X in the studied pH range. Table 4-6 provides comparison of the two models used for describing lead adsorption on Na-X zeolite. From the table, it is evident that the pseudo second order had a higher correlation to the experimental results and better described the lead adsorption onto Na-X. It can be concluded that the pH had a significant effect on sorption capacity.

Table 4-6 Pseudo first and Pseudo second order isotherm constants for adsorption of Pb^{2+} on Na-X zeolite

Initial pH	**Pseudo-first order model**	**Pseudo-second order**

	q_e (mg/g)	k_L (1/h)	R^2	q_e (mg/g)	k_H (g/mg.h)	R^2
3	15.4	1.03	0.93	17.9	0.04	0.99
4	40.6	2.41	0.96	43.3	0.06	0.98
5	43.1	2.82	0.95	46.1	0.07	0.99
6	48.3	3.52	0.91	48.9	0.11	0.97

4.4.2) Adsorption isotherms

The adsorption process is usually described through graphs known as adsorption isotherms. Adsorption isotherm is the constant-temperature equilibrium relationship between the quantity of adsorbate on adsorbent as a function of its pressure (in gas phase) or concentration (in liquid phase). The adsorbed quantity is always normalized by the mass of the adsorbent to allow comparison of different materials. The equation parameters and also the thermodynamic assumptions of equilibrium models provide a basis to understand adsorption mechanism, surface properties of the adsorbent, and its affinity toward the adsorbate. Langmuir and Freundlich models were employed to analyze Pb^{2+} adsorption isotherms.

- Langmuir model

The Langmuir model of adsorption assumes that a monolayer of adsorbate may be adsorbed on adsorbent surface before adsorption capacity is reached, and each adsorbate molecule occupies only one site. Langmuir model assumes that adsorption energy is constant and independent of surface coverage, adsorption occurs only on localized sites without lateral interactions between the adsorbate molecules, and once adsorbed, the adsorbate remains on the same adsorption site until desorbed. The Langmuir relationship is given in equation 4-6:

$$q_e = \frac{q_m a_1 C_e}{1+a_1 C_e} \qquad \text{Equation 4-6}$$

Where a_1 represents the isotherm constant ($L.mg^{-1}$) and q_m is Langmuir monolayer saturation capacity.

A dimensionless equilibrium term R**,** also known as the separation factor is used to evaluate the Langmuir constant a_1 and provides important information about the nature of the adsorption isotherm. *Table 4-7* shows the application of R factor in the evaluation of the nature of adsorption.

Table 4-7 Evaluation of separation factor (R) in Langmuir model

Separation factor, R	Adsorption performance
R>1	Unfavorable
R=1	Linear
0<R<1	Favorable
R=0	Irreversible

R values can be obtained from Langmuir isotherm constant a_1 ($L.mg^{-1}$) using equation below

$$R = \frac{1}{1+a_1 C_0} \qquad \text{Equation 4-7}$$

Where C_0 = initial concentration of lead.

- Freundlich model

Unlike the Langmuir isotherm, the Freundlich model of adsorption does not assume that adsorption capacity is reached when a monolayer of adsorbate is adsorbed, but recognizes that the adsorbent surface may contain a range of different adsorption site types, and the Langmuir equation will be valid for each. Therefore, this empirical model can be applied to non-ideal adsorption on heterogeneous adsorbents and multilayer adsorption. The Freundlich relationship is given in equation below.

$$q_e = k_F . C_e^{\frac{1}{n}} \qquad \text{Equation 4-8}$$

Where k_F ($L.mg^{-1}$) is Freundlich constant, 1/n represents Freundlich intensity parameter, and C_e ($mg.L^{-1}$) is the equilibrium concentration of adsorbate in solution.

Isotherm experiments were conducted in batch systems using different representative weights of zeolite to study the adsorption of lead onto Na-X at four different pH levels. The Langmuir and Freundlich models were used to describe the adsorption isotherms.

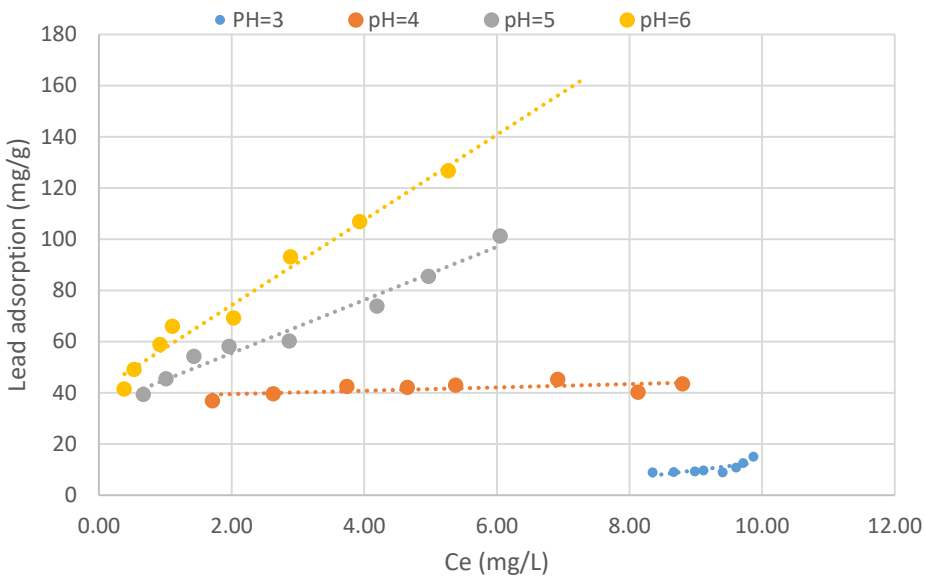

Figure 4-12 Experimental results of adsorption isotherms for Pb^{2+} on Na-X

Both Langmuir and Freundlich equations were used to describe the adsorption data with Freundlich isotherm showing better correlation with experimental results at more neutral pH and Langmuir being applicable at lower pH values (pH=4). Both models were unable to describe the adsorption data at very acidic conditions and showed a poor correlation value at pH 3.0.

Table 4-8 Adsorption constants for Freundlich and Langmuir isotherms for Pb^{2+} adsorption onto Na-X zeolite

Initial pH	**Langmuir model**			**Freundlich model**		
	q_m	**k_L**	**R^2**	**k_F**	**n**	**R^2**
3	1430	840	0.89	1.2	0.38	0.61
4	47	2.47	0.96	36.7	2.16	0.56
5	115	0.58	0.90	43.6	2.37	0.98
6	135	0.78	0.84	59.9	2.56	0.96

Desorption studies were conducted at different pH levels. The concentration of desorbed lead was below the detection limits of atomic absorption spectrophotometer. In the controlled study carried out using fly-ash based zeolite and 100 mL of DI water, no lead ion was detected after 2 hr. exposure time, therefore the desorption of Pb^{2+} to water was not significant.

4.5) Lead adsorption studies using SOD

4.5.1) The effect of adsorbent dosage

Adsorbent dosage effect on the percentage removal of Pb^{2+} is shown in Figure 4-13. It can be seen that adsorption of lead at lower concentrations (100 ppm) is favorable and the percentage removal initially increases sharply with the increase in the adsorbent dosage, and beyond a value of 3.0 g/L, the percentage removal reaches an almost constant value. This may be due to an overlapping of adsorption sites as a result of over-crowding of adsorbent particles. The percentage removal of Pb^{2+} increased from 68.0% to 98.1% for an initial concentration of 100 mg/dm^3; 23.1% to 69.8% for an initial concentration of 250 mg/dm^3; and 16.5% to 53.2% for an initial concentration of 500 mg/dm^3, with an increase in the adsorbent doses from 0.5 g/dm^3 to 5.0 g/dm^3 at room temperature (25°C) and pH 6.0. A maximum of 98.1% removal was observed for an initial lead concentration of 100 mg/dm^3 at an adsorbent dosage of 3.0 g/dm^3. Therefore, the use of a 3.0-3.5 g/dm^3 adsorbent dose is justified for treatment of up to 100 ppm lead solution.

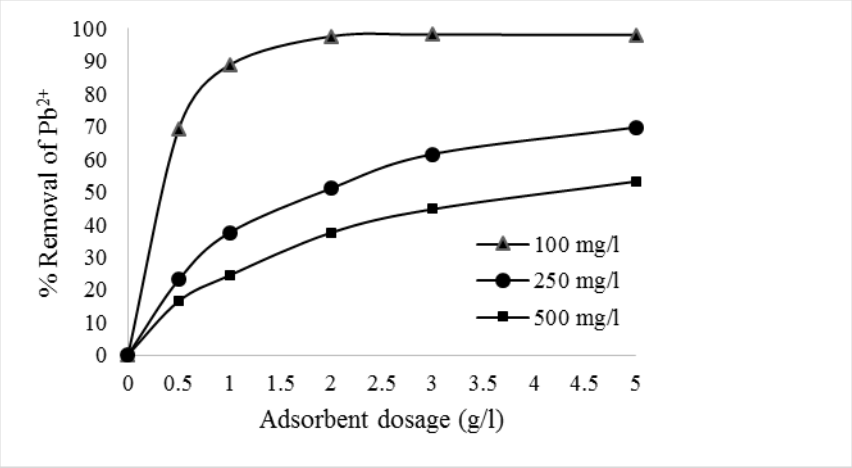

Figure 4-13 Effect of adsorbent dose on Pb(II) removal efficiency of hydroxy sodalite

4.5.2) Effect of contact time

The relationship between contact time and lead sorption onto zeolite adsorbent at different initial lead concentrations is shown in Figure 4-14. The adsorption rate was high in the first 2 hours and then slowed down. With further increase in time, the sorption kinetics decreased progressively and reached equilibrium within 6 hours for all three initial lead concentrations. The removal efficiency corresponding to equilibrium adsorption increased with decreasing initial lead concentration. The fast adsorption at the initial stage is due to the availability of an increased number of exchange sites in the zeolite structure at the beginning. The progressive increase in adsorption and, consequently, the attainment of equilibrium adsorption may be due to limited mass transfer of the adsorbate molecules from the bulk liquid phase to the external surface of zeolite adsorbent, initially and subsequently, by slower internal mass transfer within zeolite particles.

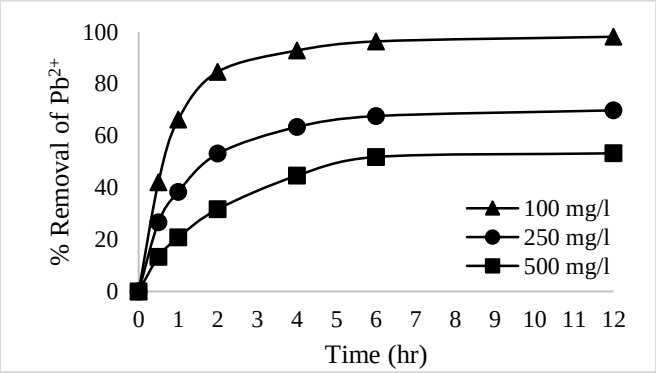

Figure 4-14 Lead ion removal efficiency (solid/liquid: 3.0 g/L) versus time

4.5.3) Effect of initial concentration of Pb^{2+} on metal uptake

It was observed that the uptake capacity of the synthetic zeolite sample (ZCFA) was higher than fly ash (CFA) in all initial Pb^{2+} concentrations. The amount of Pb^{2+} adsorption of ZCFA and CFA increased from 32.7 mg/g to 152.3 mg/g and from 7.6 mg/g to 10.3 mg/g with an increase in the initial adsorbate concentration from 100 mg/dm^3 to 1000 mg/dm^3 .The efficiency of Pb^{2+} removal is affected by the initial

concentration, with a decreasing removal capacity as the concentration increases from 100 mg/dm^3 to 1000 mg/dm^3.

Since there is a number of exchangeable sites in zeolite framework that tend to become saturated at higher Pb^{2+}/adsorbent ratios, the initial Pb^{2+} concentration provides the necessary driving force to overcome the resistance to the mass transfer of lead ions between aqueous and solid phases. The increase in initial lead concentration enhances the interaction between zeolite and Pb^{2+} ions, and therefore, higher metal uptake was observed at higher initial lead concentrations.

The increase in equilibrium adsorption capacity with increasing the initial lead concentration indicates that there are plenty of adsorption sites available for the adsorption of heavy metal ions. The increased adsorption of lead ion with the increase in agitation time may be due to reduction of boundary layer resistance to mass transfer in the bulk solution and an increased kinetic energy of hydrated lead ions. Figure 4-15 shows the metal uptake (q_e) as a function of time with an initial Pb^{2+} concentration of 500 mg/dm^3 and an adsorbent/liquid ratio of 1g/dm^3. In addition, analysis of pH as a function of time was conducted to determine the minimum time required to obtain lead adsorption equilibrium. Figure 4-15 displays the pH data for the 500 mg/dm^3 lead solutions placed in contact with 1g/dm^3 ZCFA for 10 hours. A relatively fast pH change from the initial value of 5.5 to 6.6 was observed during the first two hours followed by a slower rate of change until the final value of 7.2 was reached in 10 hours.

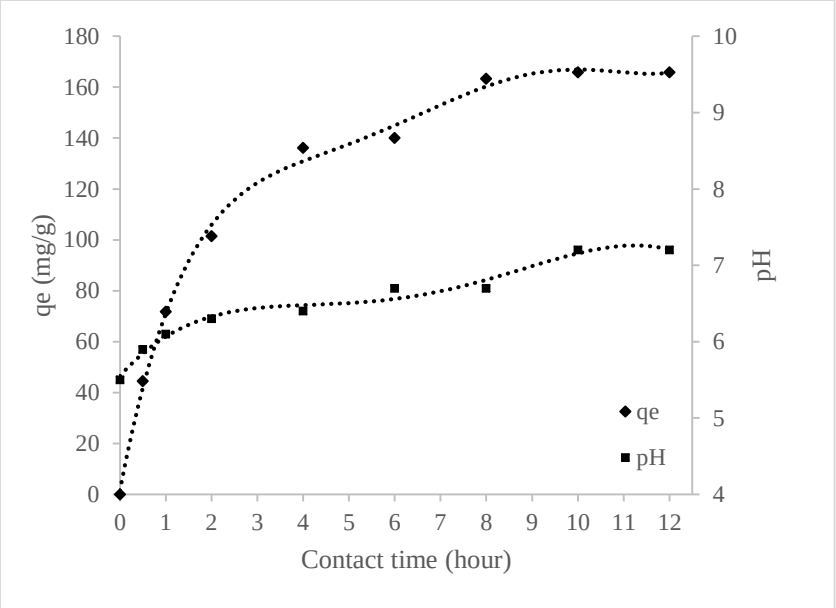

Figure 4-15 Effect of contact time on the adsorption capacity of ZCFA (sodalite) for Pb^{2+} (amount of adsorbent: 1.0 g/l, initial Pb^{2+} concentration: 500 mg/l)

The magnitudes of K_f and n show an easy separation of Pb^{2+} ions and indicate highly favorable adsorption. The slope (1/n) describes the effect of concentration on the adsorption capacity and represents the adsorption intensity. The isotherm parameters for Pb^{+2} adsorption on ZCFA are listed in Table 4-9.

Table 4-9 Isotherm model constants and correlation coefficients for adsorption of Pb^{2+} at pH=5.5

Adsorbent	Langmuir isotherm			Freundlich isotherm		
	q_m (mg/g)	K_L (L/mg)	R^2	K_f (mg/g)	n	R^2
ZCFA	153.84	0.1697	0.998	20.922	1.758	0.972

The K_f value of the Freundlich equation indicates that the zeolite has a very high adsorption capacity for lead ions in aqueous solutions. Values of n between 1 and 10 indicate efficient adsorption. The results indicate that the studied zeolite possesses a very high adsorption capacity while and a relatively slow adsorption kinetic. Langmuir model showed better compatibility (regarding the values of R^2) compared with Freundlich model. The applicability of Langmuir model is an indication of homogeneity of

adsorption sites over the adsorbent. It can be concluded that the adsorption on ZCFA surface was homogeneous.

4.5.4) Pore size modification

The modification of pore size was studied using pure synthetic A type zeolite (LTA). Activated kaolin was used as source of silica and alumina. Kaolin was passed through a No. 325 test sieve (opening: 45μm) and was activated and transformed into kaolinite in a calcination process at 900°C for 2h. The dihydroxylation reaction occurs according the following chemical route:

$$2Al_2Si_2O_5(OH)_5 \rightarrow 2Al_2Si_2O_7 + 4H_2O \qquad \text{Equation 4-9}$$

100 ml of sodium hydroxide solution (3M) was added to 3 gram of the dehydroxylated kaolin to prepare initial gel (NaOH solution 3g). The mixture was stirred using a temperature-controlled heater and mixed using a mechanical mixer at 80°C until aluminosilicate gel was formed (2 h.). Nucleation step was performed at room temperature for 96h followed by crystallization at 90°C for 3h. The precipitated zeolite crystals were washed with distilled water until a pH of 10 was achieved, dried in a vacuum oven at 90°C for 24h, ground with a SPEX 8000M mill for 5 minute and passed through a No. 325 test sieve. The dried zeolite powder was used in the silver and calcium exchange reactions.

The calcium and silver ions were introduced to the zeolite in an exchange process. Analytical grade calcium chloride ($CaCl_2$) and silver nitrate ($AgNO_3$) were used to prepare 1M aqueous solution which were then refluxed with zeolite with a solid/liquid ratio 1g: 100ml. The silver exchange process was carried out in darkroom. The exchange process was performed at 80°C for 6 h. Exchange process can proceed even in ambient temperature due to higher affinity of both Ca^{2+} and Ag^{+} ions toward exchange sites over Na^{+} ions. Calcium- and silver-exchanged zeolites were separated by simple filtration, washed

with distilled water and isopropanol, dried in a vacuum oven at 90°C for 24h., milled and were noted as Ca-A and Ag-A, respectively

The identification of the phases present was done using International Center for Diffraction Data Powder Diffraction File (ICDD-PDF 2.0). The results indicate that both calcium and silver ions tend to disperse uniformly in the zeolite framework. As can be seen in Table 4-10, cell type and space group were similar in both exchanged A type zeolites. Figure 4-16 shows the representative XRD pattern of Ca-A and Ag-A zeolite samples. Both samples were identified as a single phase zeolite.

Table 4-10 Results of XRD analysis of Ca- and Ag- exchanged zeolite A

	Cell system	***Space group***	***Crystallite size***	***Crystallinity***	***Chemical composition***	***PDF***
Ca-A	Cubic	Pm-3m (221)	108.2 nm	64.3	$Na_{7.9}Ca_{2.4}(Al_{11.8}Si_{12.2}O_{48})(H_2O)_{34.8}$	01-080-6159
Ag-A	Cubic	Pm-3m (221)	57.6 nm	59.4	$Ag_{12}(Al_{12}Si_{12}O_{48})(H_2O)_{6.7}$	01-088-2480

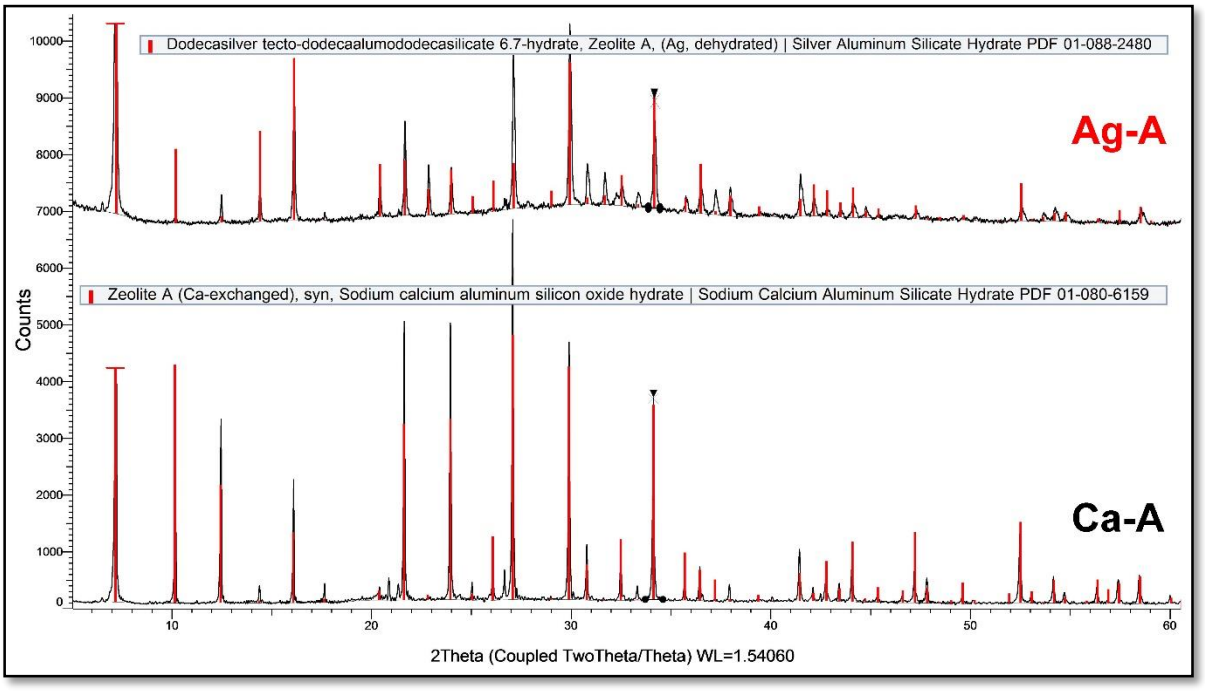

Figure 4-16The XRD pattern of Ca- and Ag-exchanged zeolite A

SEM micrographs presented in Figure 4-17 for both Ca- and Ag-exchanged zeolite A clearly show both samples have a rough surface which is an indication of high surface area. The mean diameter of synthesized zeolites were 1.6-3.8 and 0.9-2.3 µm for the Ca-A and Ag-A samples respectively.

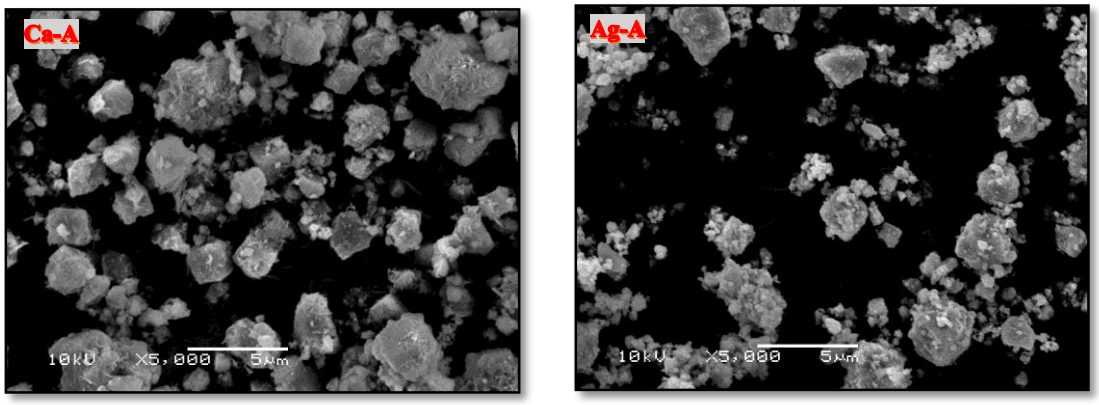

Figure 4-17SEM images of Ca-A and Ag-A, zeolite crystals

The elemental distribution of Al, Si, O, Ca, and Ag was studied using EDX mapping. Uniform distribution of Ca and Ag elements in their respective form of A type zeolite is an indication of successful exchange process. The intensity of sodium peak in calcium exchanged zeolite is low and sodium content of the silver-exchanged type is even lower which is an indication of successful exchange of cations of the synthesized precursor. In conventional synthesis method, some of the sodium are trapped in the sodalite cages of the zeolite. Since EDX method is less sensitive to those elements with atomic number below 10, the weight percent are reported in carbon- and oxygen-free basis. As can be seen in Figure 4-18, sodium, aluminum and silicon were distributed relatively uniform. Oxygen was abundant in highly crystalline areas while calcium was spread in amorphous aggregates.

Table 4-11 Elemental composition of Ca- and Ag- exchanged zeolite A

Zeolites	***Al***	***Si***	***Ca***	***Ag***	***Na***
Ca-A	34.79	43.19	14.98	-	6.86
Ag-A	17.76	26.55	2.60	52.02	1.07

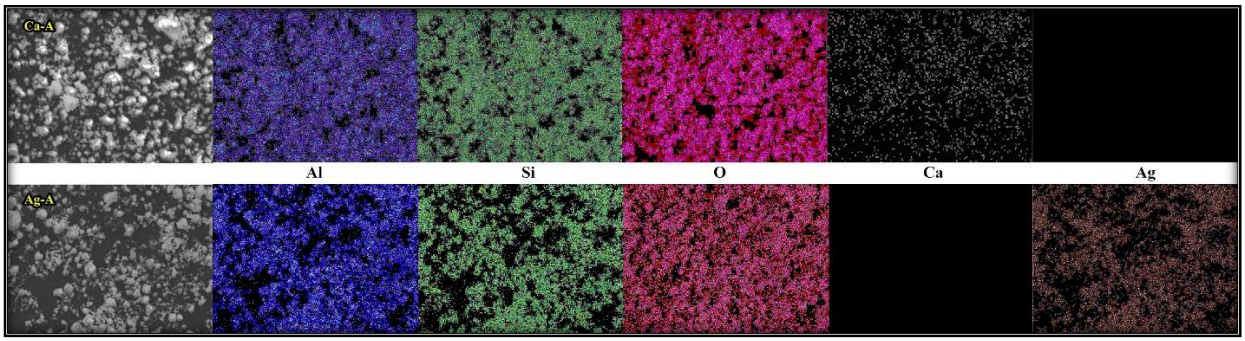

Figure 4-18EDX mapping of micro-particles of a. Ca-A and b. Ag-A, and corresponding elemental mapping of Al, Si, O, Ca, and Ag.

Figure 4-19 exhibits the N_2 adsorption and desorption isotherms at -195.9°C for zeolites Ca-A and Ag-A. According to an updated classification of physisorption isotherms, the isotherm is of type I(a) which is seen in microporous solids having mainly narrow micropores of width < 1nm. The limiting value of amount adsorbed is governed by the accessible micropore volume rather than by internal surface area. The steep uptake at very low p/p^0 is due to enhanced adsorbent-adsorptive interactions in narrow micropores. The hysteresis loop seen in the multilayer range of both samples, are associated with capillary condensation in mesopore structure as a result of metastability of the adsorbed multilayer in an open-ended pore. The narrow and steep hysteresis loop is a clear sign of delayed condensation associated with pore blocking. Desorption branch is used for mesopore size analysis, but this method is now considered to be questionable since the desorption path may be dependent on network percolation effect or pore diameter variation along single channels.

Table 4-12 gives surface area, pore volume, and average pore diameter for the Ca- and Ag-exchanged zeolite A. Micropore area and volume were calculated based on t-plot method and the total pore volume was calculated at p/p_0=0.99. Larger exchanged cation in Ag-A decreased the micropore volume. While XRD analysis confirmed that the type A framework in the resulting Ca- and Ag-exchanged zeolites maintained unchanged, α-site occupation of silver ions tend to decrease the aperture size of the zeolite and reduction of accessible path for N_2 molecules which in turn limits the access to channels. The smaller specific area seen in silver exchanged zeolite A can be attributed to the blocking of the channels.

Table 4-12 Surface area and exchange capacity of Ca- and Ag- exchanged zeolite A

	Surface area (m^2/g)		***Pore volume (cm^3/g)***		***BJH average pore diameter (nm)***		
Zeolites	BET	Micropore area [a]	Total pore volume [b]	Micropore volume[a]	Adsorption	Desorption	CEC (meq/g)
Ca-A	451.0	417.9	0.27	0.200	6.06	9.9	4.54
Ag-A	207.6	190.7	0.14	0.092	8.11	11.4	3.57

[a] calculated based on t-plot method
[b] Total pore volume at $p/p_0 = 0.96$

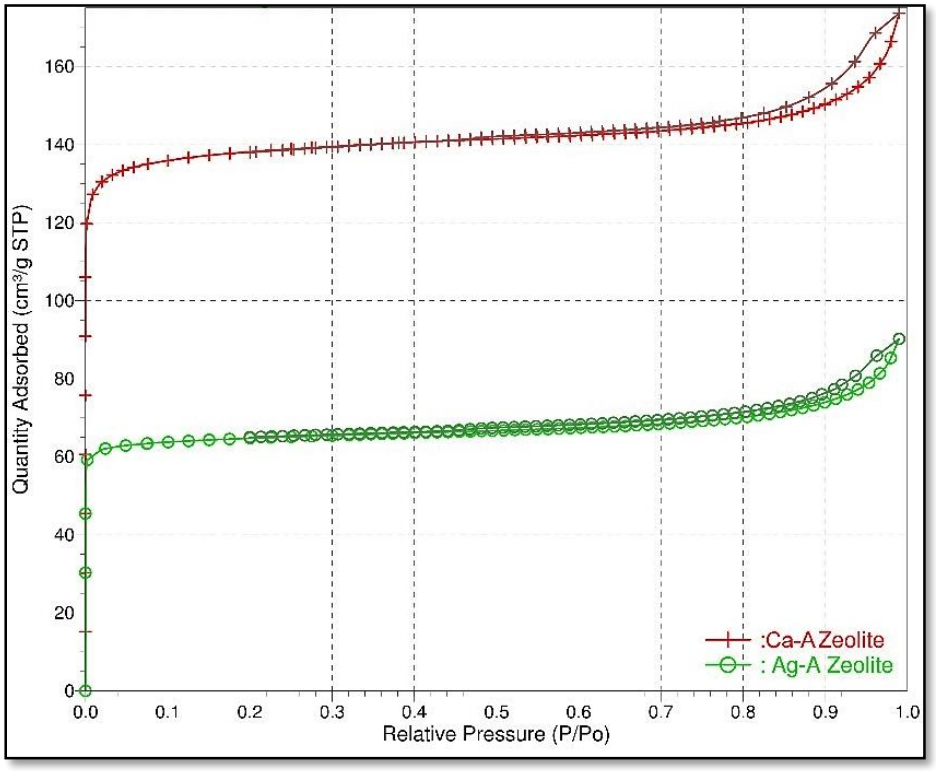

Figure 4-19 Nitrogen adsorption isotherms of zeolite Ca-A and Ag-A at -196.15 °C

X-ray photoelectron spectroscopy was performed in order to confirm the electronic states of silver and calcium in samples. shows the fully scanned spectra of Na-A and Ag-A zeolites in the range of 0–1000 eV. The elements C, Si, Al, O, and Ca were demonstrated to exist in the Ca-A zeolite and Ag, C, O, and Si were detected in the Ag-A sample. The chemical elements Si, Al, O and Na were attributed to 4A-zeolite. The binding energy of Ag $3d_{5/2}$ was found to be 368.4 eV which is higher than the values measured for the

$AgNO_3$ and Ag_2O pure compounds (368.1 eV) and could belong to Ag^+ ions . It was confirmed that Ca^2, and Ag^1 were states of calcium and silver in the Ca-A and Ag-A, respectively.

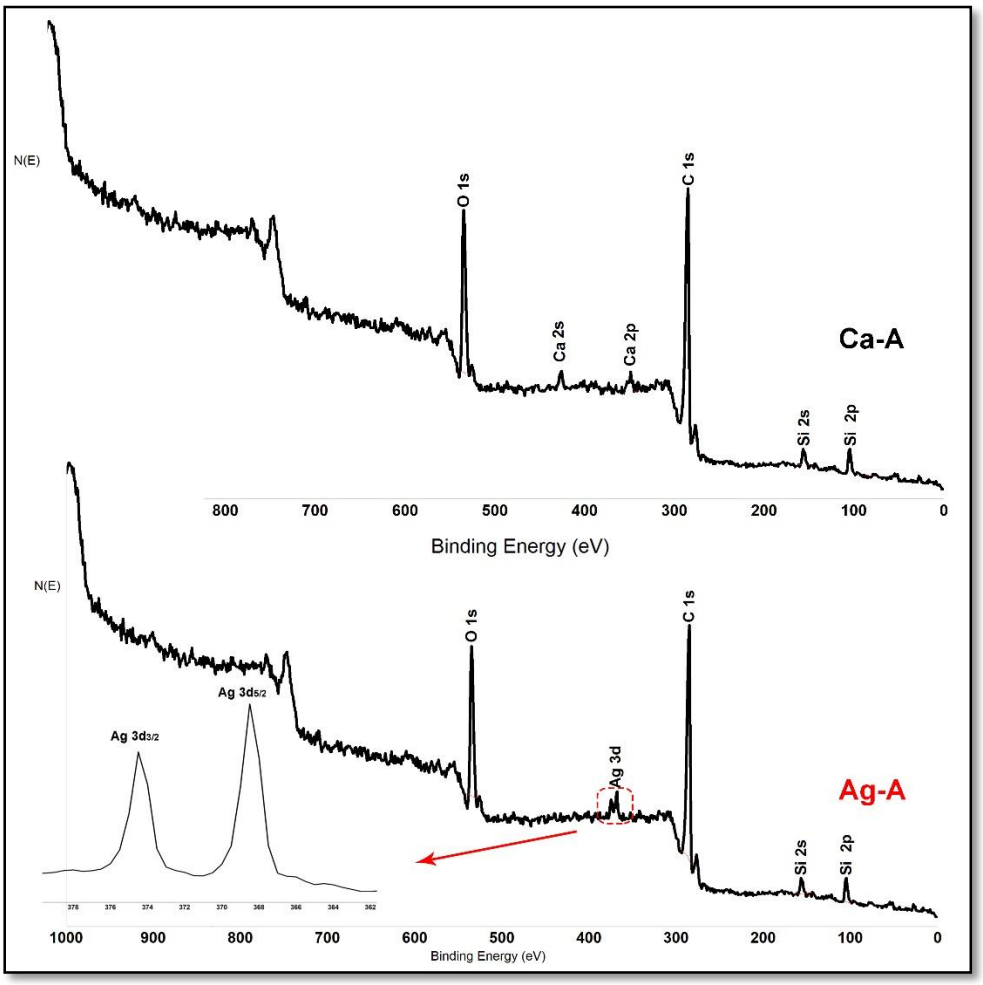

Figure 4-20 XPS analysis of Ca-A and Ag-A (top and bottom respectively)

The FTIR spectrum for the Ca-A and Ag-A zeolite samples in the range of 4000-600 cm^{-1} is given in Figure 4-21 FTIR spectra of Ca-A and Ag-A zeolite. The FTIR spectra shows a sharp peak with high intensity at 990 and 971.5cm^{-1} for the Ca-A and Ag-A samples respectively. This vibration is assigned to the T–O–T (T= Al or Si) asymmetric stretching vibration. It is observed that the peak detected at 710 and 718 cm^{-1} which can be assigned to the T–O–T symmetric stretching has less intensity compared to the asymmetric stretching of T–O–T bond in Ca-A and Ag-A, respectively. This is likely as the probability of

symmetric stretching of T–O bond is less compared to asymmetric stretching and bending. In zeolites, the water molecules are associated with cations or framework oxygen. The association of the water molecules with the cation or framework oxygen ions of a zeolite is dependent upon the openness of the structure. The broad band observed at 3360 and 3385 cm^{-1} is characteristic of hydrogen bond between the oxygen atoms of the framework and OH in water.

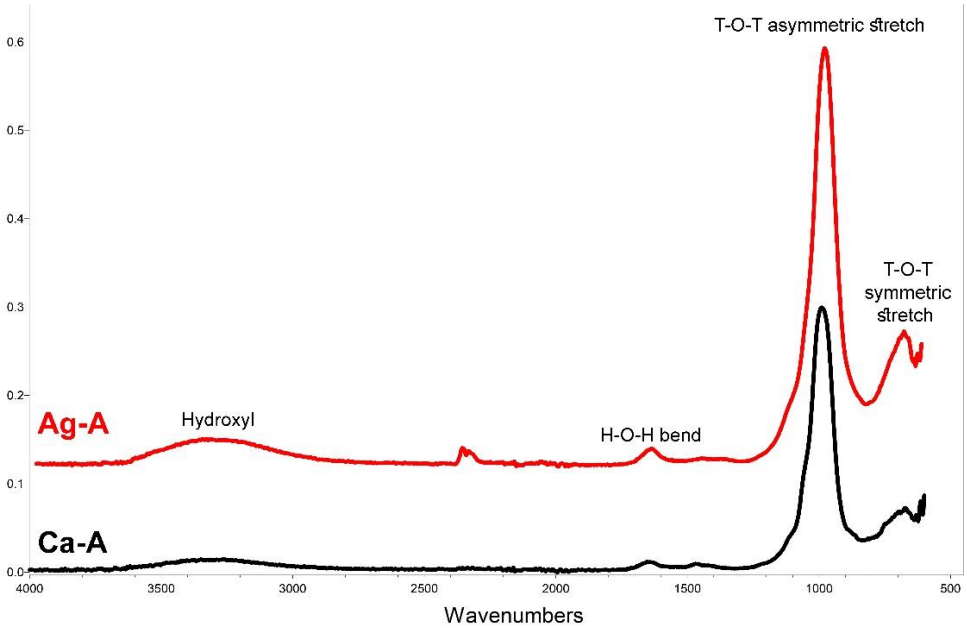

Figure 4-21 FTIR spectra of Ca-A and Ag-A zeolite

Chapter -5) Conclusions and future work

5.1) Conclusions

Cost-effective production of zeolites from fly ash provides an opportunity for effective and value added management of fly ash. Technological advances can be effective in managing fly ash, in addition to the possibility of its utilization in the synthesis of zeolites for water treatment applications. Class F fly ash was hydrothermally modified in one and two step processes to prepare zeolites with enhanced adsorption characteristics. Highly crystalline X type zeolite and hydroxy sodalite were targeted as microporous and mesoporous zeolite and were successfully synthesized using fly ash precursor by adjusting Si/Al ratio.

The chemical, mineral, morphological and thermal properties of the obtained zeolites was determined. The ammonium acetate saturation method followed by atomic absorption spectroscopy was employed for CEC measurements. Increasing the hydrothermal synthesis time up to 48 hr increased the crystallinity while the CEC value showed slight reduction after 24 hr. BET analysis revealed that the nitrogen adsorption on Na-X was type I(a) that is seen in microporous materials. The specific surface area of Na-X was found to be 424.3 m^2/g. The hydroxy sodalite adsorption isotherm was type IV with an specific surface area of 42.6 m^2/g. TG and DTA analysis revealed that the loosely bound water molecules were released from Na-X zeolite below 450K while more strongly bound water molecules where released gradually up to 1230 K where the zeolite structure collapsed. The presence of porosity, as well as high specific surface area and CEC suggests potential applications in adsorption and ion exchange applications.

Adsorption of heavy metals on the obtained fly ash-based zeolites was expected to be favorable. This was confirmed with lead adsorption experiments. The removal of Pb^{2+} with hydroxy sodalite and Na-X zeolite was investigated under various conditions. The adsorption capacity of hydroxy sodalite increased with an increase in contact time, and a 98.1% removal efficiency was observed for a solid/liquid ratio of 3.0 g/dm^3 and an initial lead concentration of 100 mg/dm^3. The Langmuir model represented the

adsorption on process sodalite better than the Freundlich model and the maximum adsorption capacity of Pb^{2+} onto hydroxy sodalite was 153.8 mg/g. The results indicate that Pb^{2+} can be adsorbed successfully in significant amounts on the modified fly ash.

Batch kinetic and isotherm studies were conducted to investigate the potential of Na-X for the removal of lead from aqueous solution. The effect of initial pH on adsorption process was investigated and pseudo first order and pseudo second order adsorption kinetics equations were used to model experimental data. Based on the kinetic experiments, the equilibrium time required for the adsorption of lead from aqueous solution by Na-X was 150 min. The pseudo second order model represented the adsorption kinetics better than the pseudo first order model. The reaction rate constants, as well as sorption capacity increased with increasing pH in the range of 3 to 6. Optimum pH for the removal of lead with initial concentration of 10 ppm was found to be 6.0. Possibility of pore size tailoring was studied in silver exchange studies. XPS studies confirmed the presence of highly dispersed cationic silver species at exchange sites of silver exchanged zeolite A.

5.2) Future work

Since zeolite pores are very narrow, the effective diffusivity in zeolite crystals is limited, which limits the application of zeolites for some applications. Targeted introduction of mesoporosity, in order to enhance the transport properties of the zeolite is desirable. Different synthetic strategies have been developed, which focus on the formation of mesopores in zeolite single crystals.

Another approach is the formation of hierarchically ordered pore structures. This can be obtained by post- treatment of parent materials or by applying novel synthesis routes. The use of surfactant mixtures and liquid crystalline templating is possible for the synthesis of zeolites with a 3D arrangement of well-defined pores of different sizes.

It is very difficult to directly compare various adsorbents based on their adsorption capacities due to inconsistency in the literature data. Sorption capacities were evaluated at different pHs (and not necessarily at the optimum pH values), adsorbent doses, temperatures, and pollutant concentration ranges. The adsorbents were used for treatment of synthetic industrial wastewater, ground water, drinking water, and actual wastewater, therefore, due to the huge difference in the types and concentrations of interfering ions, the results cannot be readily compared with each other. Although in some cases the exchange capacities of coal-based adsorbents are lower than polymeric exchange resins and activated carbon, the lower cost of coal showed great potential for its utilization for the removal of a range of pollutants from water and wastewater effluents. The properties of the coal-based adsorbents are dependent upon the production and/or conversion methods and the nature of the coal itself. Recently, extensive research efforts have been devoted to the surface modification of coal, aimed at increasing the surface area or introducing surface functional groups. Such approaches include demineralization, heat treatment, oxidation, and nitration, among others.

Chapter -6) References

1. Adamczyk, Z. and B. Bialecka (2005). "Hydrothermal synthesis of zeolites from Polish coal fly ash." Polish Journal of Environmental Studies **14**(6): 713.

2. Ahmaruzzaman, M. (2010). "A review on the utilization of fly ash." Progress in energy and combustion science **36**(3): 327-363.

3. Auerbach, S. M., et al. (2003). Handbook of zeolite science and technology, CRC press.

4. Baerlocher, C., et al. (2007). Atlas of zeolite framework types, Elsevier.

5. Bandura, L., et al. (2015). "Synthetic zeolites from fly ash as effective mineral sorbents for land-based petroleum spills cleanup." Fuel **147**: 100-107.

6. Bandura, L., et al. (2013). "Synthesis of zeolites from fly ashes–the industrial scale." Global Journal on Advances Pure and Applied Sciences **1**: 574-579.

7. Barakat, M. (2008). "Adsorption of heavy metals from aqueous solutions on synthetic zeolite." Research Journal of Environmental Sciences **2**(1): 13-22.

8. Barakat, M. (2011). "New trends in removing heavy metals from industrial wastewater." Arabian Journal of Chemistry **4**(4): 361-377.

9. Barrer, R. (1985). "Synthesis of zeolites." Studies in surface science and catalysis **24**: 1-26.

10. Belviso, C., et al. (2014). "Removal of Mn from aqueous solution using fly ash and its hydrothermal synthetic zeolite." Journal of Environmental Management **137**: 16-22.

11. Blissett, R. and N. Rowson (2012). "A review of the multi-component utilisation of coal fly ash." Fuel **97**: 1-23.

12. Bukhari, S. S., et al. (2015). "Conversion of coal fly ash to zeolite utilizing microwave and ultrasound energies: a review." Fuel **140**: 250-266.

13. Cardoso, A. M., et al. (2015). "Synthesis of zeolite Na-P1 under mild conditions using Brazilian coal fly ash and its application in wastewater treatment." Fuel **139**: 59-67.

14. Chang, H.-L., et al. (1999). "Conversion of fly ash into mesoporous aluminosilicate." Industrial & engineering chemistry research **38**(3): 973-977.

15. Chunfeng, W., et al. (2009). "Evaluation of zeolites synthesized from fly ash as potential adsorbents for wastewater containing heavy metals." Journal of Environmental Sciences **21**(1): 127-136.

16. Cundy, C. S. and P. A. Cox (2005). "The hydrothermal synthesis of zeolites: Precursors, intermediates and reaction mechanism." Microporous and Mesoporous Materials **82**(1): 1-78.

17. Dedecek, J., et al. (2009). "Effect of Al/Si substitutions and silanol nests on the local geometry of Si and Al framework sites in silicone-rich zeolites: a combined high resolution 27Al and 29Si NMR and density functional theory/molecular mechanics study." The Journal of Physical Chemistry C **113**(32): 14454-14466.

18. Deng, H. and Y. Ge (2015). "Formation of NaP zeolite from fused fly ash for the removal of Cu (ii) by an improved hydrothermal method." RSC Advances **5**(12): 9180-9188.

19. EN, B. (2012). "450-1, Fly Ash for Concrete—Definition, Specifications and Conformity Criteria." British Standards Institution.

20. Erdem, E., et al. (2004). "The removal of heavy metal cations by natural zeolites." Journal of colloid and interface science **280**(2): 309-314.

21. Franus, W. and M. Wdowin (2010). "Removal of ammonium ions by selected natural and synthetic zeolites." Gospodarka Surowcami Mineralnymi **26**: 133-148.

22. Fu, F. and Q. Wang (2011). "Removal of heavy metal ions from wastewaters: a review." Journal of Environmental Management **92**(3): 407-418.

23. Godwin, H. A. (2001). "The biological chemistry of lead." Current opinion in chemical biology **5**(2): 223-227.

24. Golbad, S., et al. "Hydrothermal synthesis of hydroxy sodalite from fly ash for the removal of lead ions from water." International Journal of Environmental Science and Technology: 1-8.

25. Grela, A., et al. (2016). "Thermal behavior and physical characteristics of synthetic zeolite from CFB-coal fly ash." Microporous and Mesoporous Materials **220**: 155-162.

26. Gupta, V. K. and I. Ali (2004). "Removal of lead and chromium from wastewater using bagasse fly ash—a sugar industry waste." Journal of colloid and interface science **271**(2): 321-328.

27. Hay, R. L. (1966). "Zeolites and zeolitic reactions in sedimentary rocks." Geological Society of America Special Papers **85**: 1-122.

28. He, K., et al. (2016). "Removal of heavy metal ions from aqueous solution by zeolite synthesized from fly ash." Environmental Science and Pollution Research **23**(3): 2778-2788.

29. Hegazy, E. Z., et al. (2014). "Removal of heavy metal quaternary cations systems on zeolite A and X mixtures prepared from local kaolin." CLEAN–Soil, Air, Water **42**(6): 775-778.

30. Hui, K., et al. (2005). "Removal of mixed heavy metal ions in wastewater by zeolite 4A and residual products from recycled coal fly ash." Journal of Hazardous Materials **127**(1): 89-101.

31. Izidoro, J. d. C., et al. (2013). "Synthesis of zeolites X and A from fly ashes for cadmium and zinc removal from aqueous solutions in single and binary ion systems." Fuel **103**: 827-834.

32. Jha, B. and D. Singh (2014). "Formation of Meso-and Micro-Pores in Fly-Ash Zeolites Using a Three-Step Activation." Acta Geotech. Slovenica **11**(1): 63-69.

33. Kitsopoulos, K. P. (1999). "Cation-exchange capacity (CEC) of zeolitic volcaniclastic materials: applicability of the ammonium acetate saturation (AMAS) method." Clays and clay minerals **47**(6): 688-696.

34. Koshy, N. and D. Singh (2016). "Fly ash zeolites for water treatment applications." Journal of Environmental Chemical Engineering **4**(2): 1460-1472.

35. Lee, M.-G., et al. (2000). "Conversion of coal fly ash into zeolite and heavy metal removal characteristics of the products." Korean Journal of Chemical Engineering **17**(3): 325-331.

36. Maesen, T. (2007). "The zeolite scene—an overview." Studies in surface science and catalysis **168**: 1-12.

37. Marcus, B. K. and W. E. Cormier (1999). "Going green with zeolites." Chem. Eng. Prog **95**(6): 47-53.

38. Margeta, K., et al. (2013). Natural Zeolites in Water Treatment-How Effective is Their Use, INTECH Open Access Publisher.

39. Mishra, P. and R. Patel (2009). "Removal of lead and zinc ions from water by low cost adsorbents." Journal of Hazardous Materials **168**(1): 319-325.

40. Mitchell, S., et al. (2015). "Structural analysis of hierarchically organized zeolites." Nature communications **6**.

41. Mondale, K., et al. (1995). "The comparative ion exchange capacities of natural sedimentary and synthetic zeolites." Minerals Engineering **8**(4): 535-548.

42. Nascimento, M., et al. (2009). "Adsorption of heavy metal cations using coal fly ash modified by hydrothermal method." Fuel **88**(9): 1714-1719.

43. Pathania, D., et al. (2013). "Separation and estimation of heavy metals on zeolitic material synthesized from fly ash by chemical modification." Ion Exchange Letters **1**: 1-6.

44. Qiu, W. and Y. Zheng (2009). "Removal of lead, copper, nickel, cobalt, and zinc from water by a cancrinite-type zeolite synthesized from fly ash." Chemical Engineering Journal **145**(3): 483-488.

45. Querol, X., et al. (2002). "Synthesis of zeolites from coal fly ash: an overview." International Journal of coal geology **50**(1): 413-423.

46. Rhoades, J. (1982). "Cation exchange capacity." Methods of soil analysis. Part 2. Chemical and microbiological properties(methodsofsoilan2): 149-157.

47. Ribeiro, F. R. (2012). Zeolites: science and technology, Springer Science & Business Media.

48. Sasaki, H., et al. (2003). "Direct hydrothermal synthesis and stabilization of high-silica mordenite (Si∶ Al= 25) using tetraethylammonium and fluoride ions." journal of materials chemistry **13**(5): 1173-1179.

49. Shih, W.-H. and H.-L. Chang (1996). "Conversion of fly ash into zeolites for ion-exchange applications." Materials Letters **28**(4): 263-268.

50. Shoumkova, A. and V. Stoyanova (2013). "Zeolites formation by hydrothermal alkali activation of coal fly ash from thermal power station “Maritsa 3”, Bulgaria." Fuel **103**: 533-541.

51. Shyam, R., et al. (2013). "Single and binary adsorption of heavy metals on fly ash samples from aqueous solution." Journal of Molecular Liquids **178**: 31-36.

52. Somerset, V. S., et al. (2005). "Alkaline hydrothermal zeolites synthesized from high SiO 2 and Al 2 O 3 co-disposal fly ash filtrates." Fuel **84**(18): 2324-2329.

53. Sublet, R., et al. (2003). "Selection of an adsorbent for lead removal from drinking water by a point-of-use treatment device." Water Research **37**(20): 4904-4912.

54. Terasaki, O., et al. (2007). "Structural study of porous materials by electron microscopy." Studies in surface science and catalysis **168**: 477-XIII.

55. Visa, M. (2016). "Synthesis and characterization of new zeolite materials obtained from fly ash for heavy metals removal in advanced wastewater treatment." Powder Technology **294**: 338-347.

56. Wang, S. and Y. Peng (2010). "Natural zeolites as effective adsorbents in water and wastewater treatment." Chemical Engineering Journal **156**(1): 11-24.

57. Wang, Y., et al. (2003). "Synthesis of zeolites using fly ash and their application in removing heavy metals from waters." Science in China Series D: Earth Sciences **46**(9): 967-976.

58. Wdowin, M., et al. (2014). "The conversion technology of fly ash into zeolites." Clean Technologies and Environmental Policy **16**(6): 1217-1223.

59. Weitkamp, J. and L. Puppe (2013). Catalysis and zeolites: fundamentals and applications, Springer Science & Business Media.

60. Wu, D., et al. (2008). "Changes of mineralogical–chemical composition, cation exchange capacity, and phosphate immobilization capacity during the hydrothermal conversion process of coal fly ash into zeolite." Fuel **87**(10): 2194-2200.

61. Xie, J., et al. (2013). "Synthesis of zeolite/aluminum oxide hydrate from coal fly ash: a new type of adsorbent for simultaneous removal of cationic and anionic pollutants." Industrial & engineering chemistry research **52**(42): 14890-14897.

62. Xu, R., et al. (2009). Chemistry of zeolites and related porous materials: synthesis and structure, John Wiley & Sons.

63. Yadanaparthi, S. K. R., et al. (2009). "Adsorbents for the removal of arsenic, cadmium, and lead from contaminated waters." Journal of Hazardous Materials **171**(1): 1-15.

64. Yao, Z., et al. (2015). "A comprehensive review on the applications of coal fly ash." Earth-Science Reviews **141**: 105-121.

65. Zabochnicka-Świątek, M. and K. Malińska (2010). "Removal of ammonia by clinoptilolite." Global NEST Journal **12**(3): 256-261.

66. Zhao, G., et al. (2010). "Sorption of heavy metal ions from aqueous solutions: a review." The Open Colloid Science Journal **4**(1).

67. Zhou, L., et al. (2014). "Zeolites developed from mixed alkali modified coal fly ash for adsorption of volatile organic compounds." Materials Letters **119**: 140-142.